remote sensing

MDPI

Article

Vegetation Greening Driven by Warming and Humidification Trends in the Upper Reaches of the Irtysh River

Honghua Cao [1,2,3], Lu Li [4], Hongfan Xu [2,3], Yuting Fan [1], Huaming Shang [1], Li Qin [1] and Heli Zhang [1,*]

[1] Institute of Desert Meteorology, China Meteorological Administration, Urumqi/Xinjiang Key Laboratory of Tree-Ring Ecology/Key Laboratory of Tree-Ring Physical and Chemical Research of China Meteorological Administration, Urumqi 830002, China; fanyt@idm.cn (Y.F.)
[2] Yunnan Key Laboratory of International Rivers and Transboundary Eco-Security, Institute of International Rivers and Eco-Security, Yunnan University, Kunming 650500, China; hongfanx@stu.ynu.edu.cn
[3] Southwest United Graduate School, Kunming 650092, China
[4] Xinjiang Meteorological Observatory, Urumqi 830002, China
* Correspondence: zhangheli@idm.cn

Highlights

What are the main findings?

- The climate in the upper reaches of the Irtysh River exhibits a warming and moistening trend, with the NDVI showing an upward trajectory. The climate's stimulating effect on vegetation is evident, while human activities exert relatively weaker impacts.
- The North Atlantic Oscillation (NAO) and Arctic Oscillation (AO) are the primary atmospheric circulation factors regulating climate and vegetation dynamics within the basin.

What are the implications of the main findings?

- As the warming and humidification process intensifies, the driving role of climate factors in vegetation growth within the basin has become increasingly prominent.
- Developing appropriate ecological measures in response to climate change is crucial.

Abstract

To effectively manage and conserve ecosystems, it is crucial to understand how vegetation changes over time and space and what drives these changes. The Normalized Difference Vegetation Index (NDVI) is a key measure of plant growth that is highly sensitive to climate variations. Despite its importance, there has been limited research on vegetation changes in the upper sections of the Irtysh River. In our study, we combined various datasets, including NDVI, temperature, precipitation, soil moisture, elevation, and land cover. We conducted several analyses, such as Theil–Sen median trend analysis, Mann–Kendall trend and mutation tests, partial correlation analysis, the geographical detector model, and wavelet analysis, to reveal the region's pronounced warming and moistening trend in recent years, the response relationship between NDVI and the climate, and the primary drivers influencing NDVI variations. We also delved into the spatiotemporal evolution of NDVI and identified key factors driving these changes by analyzing atmospheric circulation patterns. Our main findings are as follows: (1) Between 1901 and 2022, the area's temperature rose by 0.018 °C/a, with a noticeable increase in the rate of warming around 1990; precipitation increased by 0.292 mm/a. From 1950 to 2022, soil moisture exhibited a steady increase of 0.0002 m^3 m^{-3}/a. Spatial trend distributions indicated that increasing trends in temperature and precipitation were evident across the entire region, while trends in soil moisture showed significant spatial variation. (2) During 1982 to 2022, the vegetation greening trend was 0.002/10a, indicating a gradual improvement in vegetation growth in

Check for updates

Academic Editors: Chung-Te Chang and Junhu Dai

Received: 2 December 2025
Revised: 23 January 2026
Accepted: 23 January 2026
Published: 2 February 2026

Copyright: © 2026 by the authors. Licensee MDPI, Basel, Switzerland. This article is an open access article distributed under the terms and conditions of the Creative Commons Attribution (CC BY) license.

the study area. The spatial distribution of monthly average NDVI values revealed that the main growing season of vegetation spanned April to November, with peak NDVI values occurring in June–August. Combined with serial partial correlation and spatial partial correlation analysis, temperatures during April to May effectively promoted the germination and growth of vegetation, while soil moisture accumulation from June to August (or January to August) effectively met the water demand of vegetation during its growth process, with a significant promoting effect. Geographical detector results demonstrate that temperature exhibits the strongest explanatory power for NDVI variation, whereas land cover has the weakest. The synergistic promotional effect of multiple climatic factors is highly pronounced. (3) Wavelet analysis revealed that the periodic characteristics of NDVI and climate variables over a 2–15-year timescale may have been associated with the impacts of atmospheric circulation. Taking NDVI and climatic factors from June to August as an example, before 2000, temperature was the dominant influencing factor, followed by precipitation and soil moisture; after 2000, precipitation and soil moisture became the primary drivers. The North Atlantic Oscillation (NAO) and Arctic Oscillation (AO) were the primary atmospheric circulation patterns influencing vegetation variability in the region. Their effects were reflected in the inverse relationship observed between NAO/AO indices and NDVI, with typical phases of high and low NDVI closely corresponding to shifts in NAO and AO activity. This study helps us to understand how plants have been changing in the upper parts of the Irtysh River. These insights are critical for guiding efforts to develop the area in a way that is sustainable and beneficial for the environment.

Keywords: upper reaches of the Irtysh River; NDVI; warm and humidification trend; geographical detector; atmospheric circulation

1. Introduction

Climate change is accelerating globally, with extreme weather events occurring more frequently and posing substantial challenges to human societies and natural ecosystems. Global warming has led to increased occurrences of heatwaves, droughts, and floods, and is undermining ecosystem stability, threatening biodiversity, compromising food security, and affecting the sustainability of human development [1–4]. Under ongoing climate fluctuations, vegetation systems are experiencing degradation in their capacity to provide key ecosystem services, including the regulation of material and energy flows, conservation of water, and control of wind erosion and sand movement [5–7]. These impacts are especially pronounced in arid and semi-arid regions, where vegetation degradation has become a widespread problem [8,9]. Given these conditions, systematic investigation of vegetation dynamics in these regions holds considerable scientific significance. Such research can improve our understanding of vegetation responses to climate change in ecologically vulnerable areas, provide a basis for optimizing ecological management practices, and contribute to the maintenance of ecosystem stability.

The development of satellite and remote sensing technologies has made it much easier to monitor vegetation over large areas and long time periods. Remote sensing platforms such as Landsat, MODIS, AVHRR, and SPOT offer different advantages in terms of spatial, temporal, and spectral resolution, and these have become important tools for vegetation monitoring at both regional and global scales [10–14]. Using data from these platforms, researchers have developed a variety of vegetation indices for monitoring purposes. Among the most commonly used are the Normalized Difference Vegetation Index (NDVI), Ratio

Vegetation Index (RVI), Difference Vegetation Index (DVI), Enhanced Vegetation Index (EVI), and Leaf Area Index (LAI) [15–17].

The integration of multi-source remote sensing data has also improved temporal resolution and observation continuity, offering benefits such as broad spatial coverage, frequent revisit times, and a range of monitoring indicators [18]. This allows for a better understanding of vegetation growth processes and the environmental factors influencing them. Multi-source data fusion is now commonly used [19], producing various derivative products—for example, NDVI datasets generated by combining AVHRR and MODIS observations [20,21]. NDVI does have limitations, including saturation in densely vegetated areas and sensitivity to soil background and atmospheric effects [22,23]. However, it remains among the most frequently used vegetation indicators because of its straightforward calculation, reliability, and solid physical basis [24,25], making it a key tool in vegetation monitoring and ecological studies.

Climatic factors drive vegetation growth and ecological processes. Temperature and precipitation are the two main meteorological variables that directly affect vegetation phenology and growth [26,27]. Soil moisture provides the immediate water source for plants and is important for supporting vegetation growth and reducing environmental stress [28,29]. Research has demonstrated that rising temperatures can lead to earlier greening and longer growing seasons in high-altitude regions [30]. In arid and semi-arid areas, precipitation represents the primary water input and generally exerts a stronger effect on vegetation growth compared to temperature [31]. Since the early 2000s, accelerated global warming has increased regional evapotranspiration, which has further amplified the importance of water as a limiting factor for vegetation development. This trend is more prominent in arid and semi-arid inland regions, where moderate precipitation can effectively alleviate vegetation drought stress, and its regulatory role in vegetation growth has been further amplified [32,33]. In addition, soil moisture deficit directly inhibits vegetation photosynthesis and nutrient uptake, resulting in hindered vegetation growth and a significant decline in ecosystem productivity [34]. Given the complex regulatory effects of climatic factors (temperature and precipitation) and soil moisture on vegetation dynamics in arid and semi-arid regions, as well as the sensitivity and vulnerability of vegetation ecosystems in these regions under the background of global climate change, research on vegetation dynamic assessment has become a hotspot in arid and semi-arid areas.

As one of the major water systems of the Altai Mountains, the Irtysh River is an important transnational river in Central Asia [35]. Its upper reaches are located in Altay, Xinjiang, China, with a drainage basin area of 4.8×10^4 km^2, belonging to a typical inland river basin in the arid region. This region contains extensive forest and water resources and plays an important role in transboundary water allocation, ecological conservation, and water resource management, as well as supporting sustainable agricultural and forestry development [36]. However, research on long-term climate variability and vegetation dynamics in the upper Irtysh River basin has been limited, particularly regarding how these factors interact with each other. In this study, we examine the relationship between vegetation and both climatic and non-climatic factors in the region and quantify the relative contributions of key climatic factors.

The main objectives of this study are as follows: (1) to characterize the spatiotemporal variations in temperature, precipitation, and soil moisture in the upper Irtysh River basin over recent years, and to assess whether there is evidence of a warming and wetting trend in the region; (2) to determine the long-term variation patterns in NDVI in the study area; how temperature, precipitation, soil moisture, elevation, and land cover influence NDVI dynamics; and the explanatory power of these different factors for NDVI; And (3) to determine how atmospheric circulation patterns—such as the North Atlantic Oscillation (NAO)

and Arctic Oscillation (AO)—affect regional climate evolution and the dynamic changes in vegetation growth. This study contributes new insights into the climate–vegetation relationships in the upper reaches of the Irtysh River and provides data support for developing scientifically grounded ecological protection policies.

2. Materials and Methods

2.1. Study Area

The Irtysh River originates in the Altai Mountains of Xinjiang, China. Its main stream flows northwestward along the southern foothills of the Altai Mountains, leaves China at the Beiwan section of Habahe County, and eventually enters Kazakhstan [37]. The study area encompasses the upper reaches of the Irtysh River within Chinese territory (Figure 1a), spanning 85°31′–90°29′ E and 46°50′–49°09′ N, with a drainage basin area of 4.8 × 10^4 km^2 and a main channel length of 633 km.

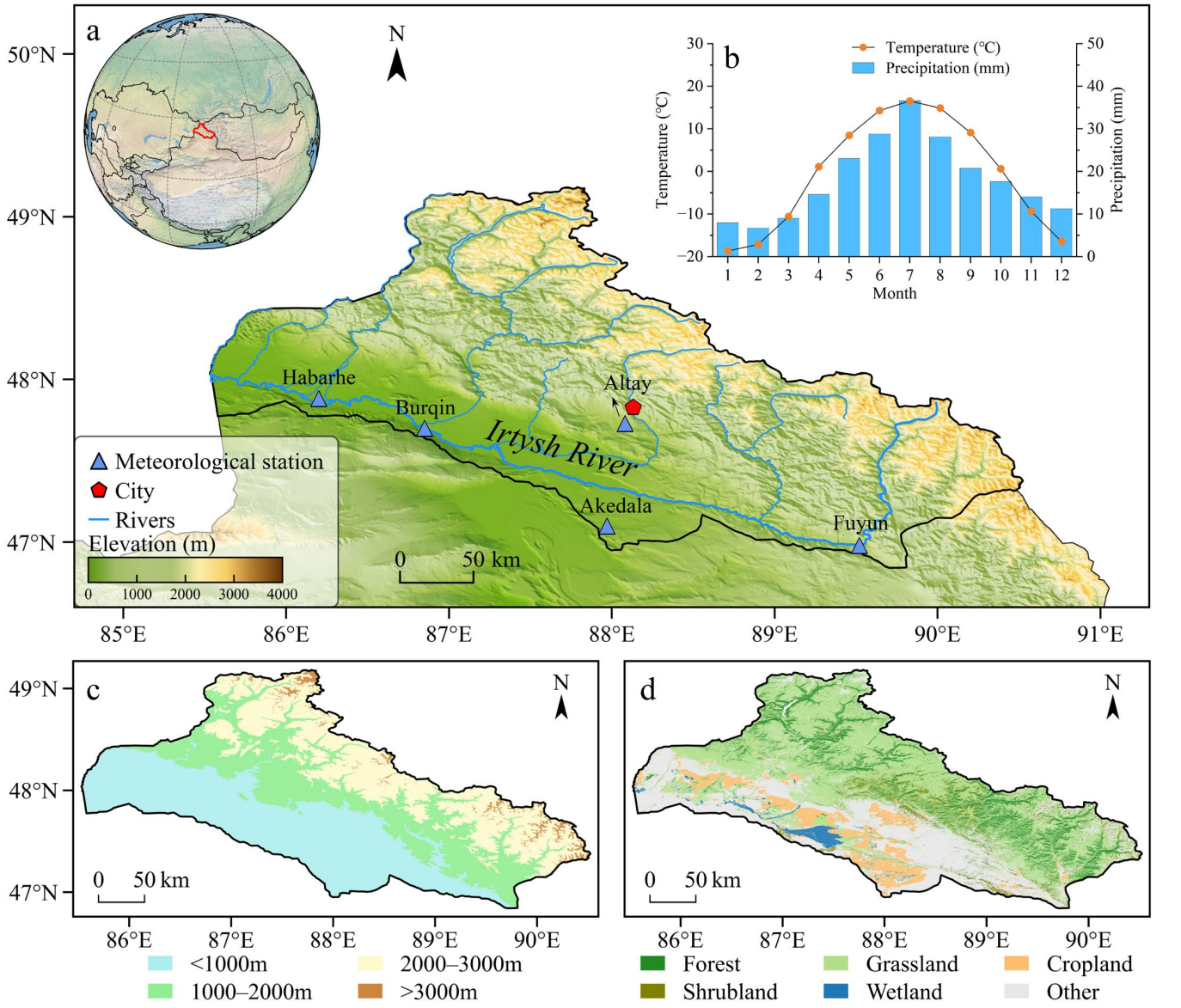


Figure 1. (**a**) Overview of the study area; (**b**) multi-year monthly average temperature and total precipitation in the study area; (**c**) altitudinal gradient in the study area; (**d**) land cover in the study area.

The average elevation of the basin is 1790 m, with higher elevations in the northeast and lower elevations in the southwest (Figure 1c) [38]. The upper Irtysh River basin exhibits a temperate continental climate and is predominantly influenced by westerly winds [38]. The mean annual temperature is around 0 °C, while annual precipitation ranges from 180 to 260 mm. July is usually the warmest month, whereas January is the coldest. Summer precipitation (June–August) is relatively abundant, accounting for about 40% of the annual total, whereas precipitation in winter and spring is relatively low (Figure 1b). The northern part is predominantly covered by forests and grasslands, while scattered croplands are distributed in the southern part (Figure 1d). Other types in Figure 1d primarily refer to bare ground, water body, or permanent snow and ice.

Runoff in the basin is mainly supplied by precipitation, snowmelt, and glacial meltwater. The flood season begins in spring, with peak discharge typically occurring between April and June. The region is characterized by pronounced temperature fluctuations, strong evapotranspiration, and high levels of solar radiation. Moisture sources are dominated by the Atlantic Ocean, with occasional and minor contributions from the Arctic Ocean. Due to orographic uplift associated with the surrounding mountains, the basin receives adequate precipitation and supports rich forest resources. Vegetation is dense in low-altitude river valleys and forest belts with sufficient water availability, while coverage decreases considerably in high-altitude and cold areas. This pronounced spatial heterogeneity along elevational gradients makes the region an ideal natural laboratory for investigating climate–vegetation interactions.

2.2. Data Sources

2.2.1. NDVI Data

This study employs the globally consistent NDVI dataset (1982–2022) with half-monthly and 1/12° spatial resolution released by Li et al. [20]. The dataset accounts for satellite orbital drift and sensor degradation, thereby reducing long-term observational uncertainties. Through pixel-level random forest fusion, the temporal span of the GIMMS NDVI3g dataset and high-quality global Landsat NDVI samples—together with MODIS NDVI (MOD13C1)—was extended to 2022. A quality-control layer provided with the dataset was applied as recommended, substantially improving data reliability. Owing to its moderate spatial resolution, accuracy, and long time series, this dataset has been widely used in studies of vegetation productivity, land-use change, and ecological restoration. NDVI data for the study area were extracted and downloaded via the Google Earth Engine (GEE) platform, and monthly NDVI values were generated using the maximum-value composite method. To reduce noise in sparsely vegetated regions, a threshold of 0.1 was adopted, and pixels with NDVI values below this threshold were excluded from statistical analyses. Given its strong performance and data quality, this dataset has been extensively validated and applied in regional and global vegetation change research, demonstrating reliable and robust results [39–42].

2.2.2. Climate and Other Data

Climate data for this study are obtained from the Chinese 1 km (0.0083°) resolution monthly precipitation and temperature datasets developed by Peng et al., spanning from 1901 to 2024 [43–45]. These datasets integrate global climate data (temperature and precipitation) at 0.5° resolution from the CRU and high-resolution global climate data from WorldClim. The Delta spatial downscaling method is used to produce high-precision downscaled data specifically for China. The dataset is validated through point-to-point comparison with observations from 496 independent meteorological stations, significantly enhancing its accuracy and reliability. Precipitation data are stored in 0.1 mm increments

and temperature data are stored in 0.1 °C increments; users should multiply by 0.1 to convert to standard units. Compared to traditional meteorological reanalysis products (e.g., CRU 0.5°, ERA5 0.25°, and GLDAS 0.25°), this dataset provides higher spatial resolution. The dataset covers the period from 1901 to 2024 and is regularly updated through continuously optimized algorithms. Data are publicly accessible. By incorporating Digital Elevation Models (DEMs) to correct for topographic effects, this dataset is particularly useful for studying regional warming and wetting trends. Previous studies have applied it to investigations of climate change and vegetation dynamics [46,47], such as works examining the relationships between NDVI and GPP dynamics in response to climate variables [48,49].

Soil moisture data were obtained from the ERA5 reanalysis dataset. ERA5 is produced by the European Centre for Medium-Range Weather Forecasts (ECMWF) and employs advanced data assimilation techniques to improve model performance, providing high spatiotemporal resolution with global coverage. Data are available from 1950 onward [50]. In this study, we used monthly soil moisture data from 1950 to 2024 at a spatial resolution of 0.1° × 0.1°, focusing on the Level 1 layer (0–7 cm depth). This layer corresponds to shallow soil moisture near the surface and responds to surface water inputs from precipitation, snowmelt, ice melt, and runoff processes. Soil moisture data at this depth are important for understanding vegetation growth, ecological dynamics, and interactions between the land surface and atmosphere.

Elevation data were derived from the SRTM 90 m dataset, and land cover data were obtained from the GlobeLand30 30 m land cover product. A summary of the data used in this study is provided in Table 1. Although bilinear interpolation tends to smooth out local extrema in the original data, it remains a relatively good sampling approach. Given the inherent characteristics of the data, meteorological factors (temperature, precipitation, etc.) and NDVI typically exhibit strong spatial continuity. Bilinear interpolation is thus more aligned with the spatial evolution patterns of these variables. This study resampled gridded data using bilinear interpolation to achieve a spatial resolution of 1/12° for temperature, precipitation, and soil moisture data, consistent with NDVI. Elevation and land cover data were resampled to 1/12° resolution using the nearest neighbor method.

Table 1. Data information.

Data	Period/Time	Spatial Resolution	Temporal Resolution	Source
NDVI	1982–2022	1/12°	15-day	Earth System Science Data (https://zenodo.org/records/8253971, accessed on 8 October 2025)
Precipitation	1901–2022	1/120°	1-Month	National Tibetan Plateau/Third Pole Environment Data Center (http://data.tpdc.ac.cn)
Temperature	1901–2022	1/120°	1-Month	National Tibetan Plateau/Third Pole Environment Data Center (http://data.tpdc.ac.cn)
Soil moisture	1950–2022	1/10°	1-Month	European Centre for Medium-Range Weather Forecasts (https://cds.climate.copernicus.eu/datasets/reanalysis-era5-land-monthly-means, accessed on 8 October 2025)
Elevation	-	90 m	-	https://dwtkns.com/srtm/, accessed on 8 October 2025
Land Cover	2020	30 m	-	National Earth System Science Data Center, National Science & Technology Infrastructure of China (http://www.geodata.cn)

2.2.3. Supplementary Data

As the study area lies on the eastern edge of Central Asia's arid and semi-arid zones, it is governed by the mid-latitude westerlies. Atmospheric circulation is dominated by westerly winds [51], with moisture primarily sourced from the North Atlantic and its transport systems [52], playing a pivotal role in water balance and climate variability. To investigate the external climatic drivers of vegetation growth changes in the upper Irtysh River region, the AO and NAO were examined from 1982 to 2022. These indices were analyzed alongside the NDVI over the same period to reveal the long-term modulating effects of large-scale circulation anomalies on regional vegetation dynamics. The AO describes variations in atmospheric circulation patterns at mid-to-high latitudes in the Northern Hemisphere. It influences polar cold air activity and affects the trajectories of mid-latitude weather systems. Decadal-scale variations in sea surface temperatures over the North Atlantic region characterize the NAO. The NAO influences the climate of the Irtysh River basin by affecting the transport of energy and moisture by the westerlies across the Eurasian continent; this influence subsequently modulates ecosystem processes in the region. This study incorporates these atmospheric circulation indices as auxiliary explanatory variables, aiming to elucidate the underlying climate mechanisms driving inter-annual vegetation variability by assessing their correlation with NDVI time series.

In addition to these data, we use NCEP/NCAR reanalysis data, which provide monthly atmospheric circulation fields starting from 1948. The dataset includes parameters such as wind speed, specific humidity, and barometric pressure, which together describe atmospheric circulation characteristics at both global and regional scales. From the 850 hPa wind field and moisture data, we examine patterns of moisture transport during periods of extreme vegetation growth in the upper Irtysh River basin (defined as periods with extremely high or low NDVI values). The enhanced vegetation growth observed during these periods could be related to anomalies in large-scale atmospheric circulation patterns.

2.3. Statistical Analysis

2.3.1. Trend Analysis

The Theil–Sen slope estimation is robust to outliers and does not assume a particular data distribution. This method is suitable for long-term trend analysis. The Mann–Kendall (MK) test is often used in conjunction with Theil–Sen estimation to evaluate the statistical significance of detected trends [53,54].

In this study, we used the MK test to analyze trends in the three gridded time series. When Sen's slope was positive, this indicated an increasing trend for that variable at the grid cell; a negative slope indicated a decreasing trend. We assessed the significance of trends using p-values as the criteria. A trend was considered statistically significant at the 95% confidence level if $p < 0.05$; otherwise, it was regarded as non-significant ($p \geq 0.05$). This approach allowed us to characterize the spatial distribution of changes throughout the study region and determine which locations showed significant trends over time.

The calculation formulas for the Theil–Sen slope estimation and MK trend test are below.

For a time series $X = \{x_1, x_2, \ldots, x_n\}$, the slope is estimated as:

$$Slope = \text{median}\left(\frac{x_j - x_i}{j - i}\right), \forall j > i \quad (1)$$

x_i and x_j denote the i-th and j-th values in the time series X, respectively; "median" represents the median value; and "Slope" denotes the slope. A slope > 0 and a slope < 0 indicate that the time series X shows an increasing trend and a decreasing trend, respectively, over the study period.

For the time series $X = \{x_1, x_2, \ldots, x_n\}$, the sign function sgn is defined as follows:

$$sgn(x_j - x_i) = \begin{cases} 1, x_j - x_i > 0 \\ 0, x_j - x_i = 0 \\ -1, x_j - x_i < 0 \end{cases} \quad (2)$$

We construct the statistic S as follows:

$$S = \sum_{i=1}^{n-1} \sum_{j=i+1}^{n} sgn(x_j - x_i) \quad (3)$$

When $n \geq 8$, the statistic S approximately follows a normal distribution. Without considering the presence of tied data points in the time series, its mean value satisfies $E(S) = 0$ and its variance is given by $Var(S) = n(n-1)(2n+5)/18$.

We construct the standardized test statistic Z as follows:

$$Z = \begin{cases} \frac{S-1}{\sqrt{Var(S)}}, & S > 0 \\ 0, & S = 0 \\ \frac{S+1}{\sqrt{Var(S)}}, & S < 0 \end{cases} \quad (4)$$

where $Var(S)$ denotes the variance in S. Assuming a significance level α, if $|Z| > Z_{1-\alpha/2}$, it indicates that the variation trend of the time series is significant (significantly increasing or decreasing). $Z_{1-\alpha/2}$ is the value corresponding to the standard normal distribution table at the confidence level α. When the absolute value of Z is greater than 1.65, 1.96, and 2.58, it means the trend has passed the significance test at the confidence levels of 90%, 95%, and 99%, respectively.

Linear regression was used to fit time series data for NDVI, temperature, precipitation, and soil moisture, which enabled us to calculate inter-annual trends in each variable. This approach allowed us to assess the long-term patterns and directional trends of these variables over time.

2.3.2. Mann–Kendall Mutation Test

The Mann–Kendall (MK) mutation test is a commonly used climatic diagnostic method for determining whether abrupt changes exist in climatic time series and for detecting the time of their occurrence [55]. For a time series $X = \{x_1, x_2, \ldots, x_n\}$, a statistic S_k is defined, where S_k represents the cumulative number of cases where the j-th sample $x_j > x_i (1 \leq i \leq j)$:

$$S_k = \sum_{j=1}^{k} r_j \ , \ r_j = \begin{cases} 1, & x_j > x_i \\ 0, & x_j \leq x_i \end{cases} (i = 1, 2, \ldots, j; k = 1, 2, \ldots, n) \quad (5)$$

Assuming that the time series is random and independent, the mean and variance of S_k are given by:

$$E(S_k) = \frac{k(k-1)}{4}, \quad Var(S_k) = \frac{k(k-1)(2k+5)}{72} \ 1 \leq k \leq n \quad (6)$$

We standardize S_k as follows:

$$UF_k = \frac{[S_k - \mathrm{E}(S_k)]}{\sqrt{Var(S_k)}} \quad (7)$$

where $UF_1 = 0$. Given a significance level α, if $|UF_k| > U\alpha$, it indicates a significant trend change in the sequence. All UF_k values can form a curve. This method is applied to the

reverse sequence, where the reverse sequence $x_n, x_{n-1}, \ldots, x_1$ is denoted as $x'_1, x'_2, \ldots, x'_n$. $\widetilde{r}_j$ represents the cumulative count of cases where the j-th sample $x_j > x_i$ ($j \leq i \leq n$). When $j' = n + 1 - j$ and $\widetilde{r}_j = r'_j$, the UB_k of the reverse sequence is given by:

$$UB_k = -UF_k, k' = n + 1 - j \ldots j, j' = 1, 2, \ldots n \quad (8)$$

where $UB_1 = 0$. UB_k is not equal to the negative value of UF_k, but is calculated based on the reverse sequence.

2.3.3. Partial Correlation Analysis and Geographical Detector Model

Multiple climatic factors influence vegetation changes, including temperature, precipitation, and soil moisture. These factors exhibit a certain degree of autocorrelation, which must be eliminated before assessing their impact on NDVI. This study employs partial correlation analysis to investigate the partial correlation between NDVI and temperature, precipitation, and soil moisture, using *t*-tests to evaluate the significance of the partial correlation coefficients [56].

The geographical detector is an open-source spatial data analysis model that assesses the similarity of spatial distributions between two variables based on spatial hierarchical heterogeneity [57]. We selected the drivers from Table 1 and utilized the factor detector and interaction detector to analyze the underlying drivers of vegetation dynamics.

2.3.4. Wavelet Analysis

Wavelet analysis, particularly the Continuous Wavelet Transform (CWT), decomposes time series signals into wavelet functions across multiple scales to reveal local signal features at different temporal scales. The method exhibits good time–frequency localization characteristics, enabling the capturing of local time–frequency properties in signals by applying scale transformations and time shifts [58,59]. We selected Morlet wavelets in this study to identify and analyze potential quasi-periodic oscillations in vegetation and climate time series, which helped to reveal their dynamic time–frequency characteristics.

Cross-wavelet transform (XWT) combines the advantages of wavelet analysis and cross-spectral analysis, allowing us to examine the co-oscillation features and their significance between two time series in the time–frequency domain [60]. Wavelet coherence analysis (WTC) normalizes the wavelet spectrum, thereby improving sensitivity to low-energy signals [61]. This normalization provides a more reliable measure of consistency and correlation between two time series at different time scales.

We apply wavelet analysis to examine correlations between vegetation changes and climatic factors (temperature, precipitation, and soil moisture) in the Irtysh River basin across different time scales and frequencies. Our objective is to characterize how vegetation responds to climatic fluctuations and to determine the mechanisms responsible for these responses.

3. Results

3.1. Spatiotemporal Variation Characteristics of Climatic and Hydrological Elements

In the study area, the average temperature was relatively high in the low-altitude southern regions (Figure 2a) and low in the high-altitude northern and northeastern regions. Sen-slope analysis revealed a significant increasing trend ($p < 0.05$) across all pixel areas (Figure 2b): the highest warming amplitude was observed in the easternmost and westernmost parts, followed by a slightly lower amplitude in the northern region, and the lowest in the central and southern regions. In terms of precipitation (Figure 2c,d), the annual total precipitation was the highest in the northwest and relatively low in the

eastern and southeastern parts of the study area. The vast majority of areas showed a significant upward trend. Regarding soil moisture content (Figure 2e,f), it was relatively high in the high-altitude northern and northeastern regions and low in the low-altitude southern regions. Most areas demonstrated an upward trend, with a small portion showing a downward trend. The northwestern region exhibited a more significant increase in soil moisture content.

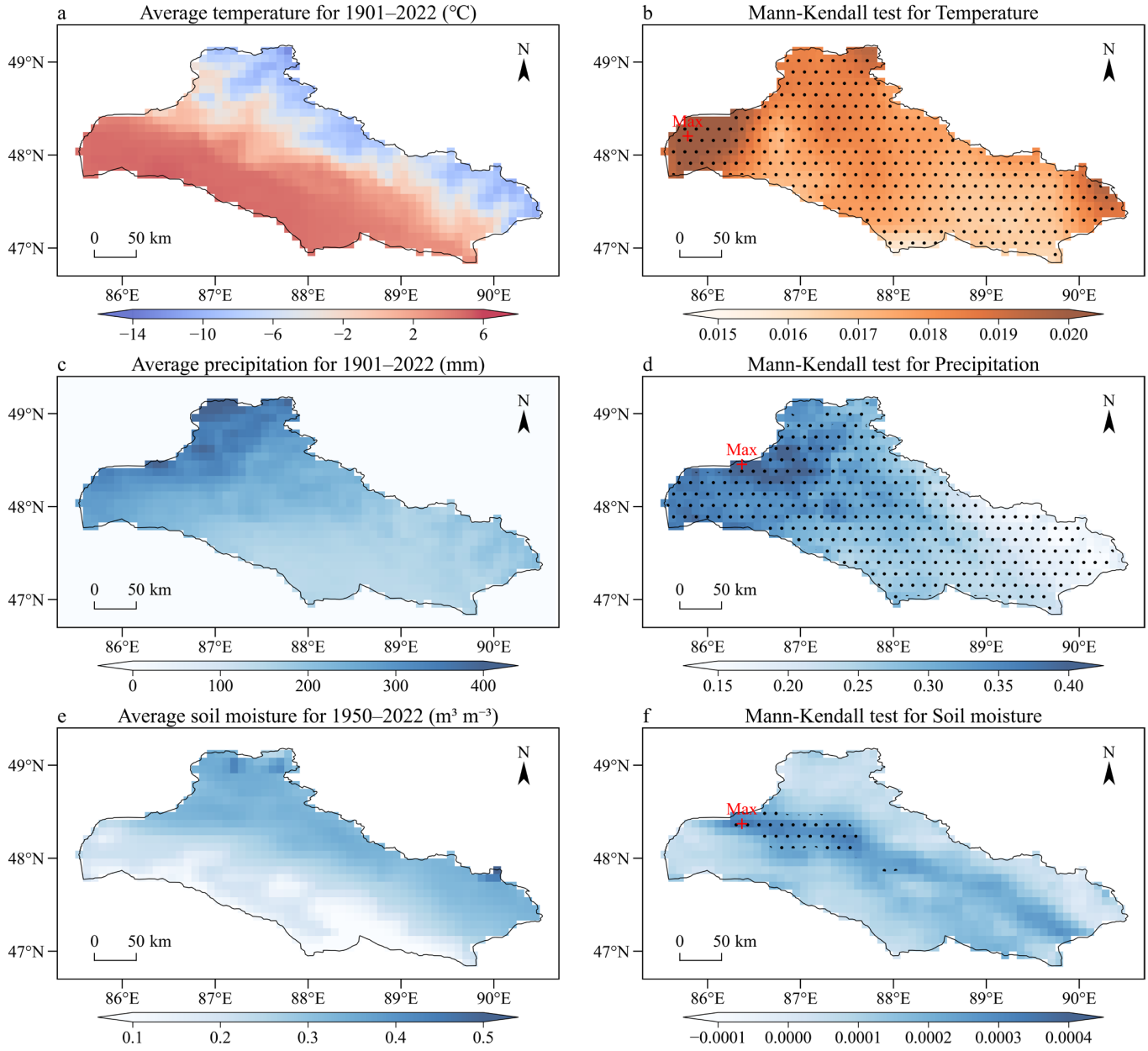


Figure 2. Spatial distribution and trend analysis of long-term average temperature, annual precipitation, and soil moisture. (**a**) Spatial distribution of average annual temperature during 1901–2022; (**b**) Mann-Kendall test for temperature; (**c**) spatial distribution of average annual total precipitation during 1901–2022; (**d**) Mann-Kendall test for precipitation; (**e**) spatial distribution of average soil moisture during 1950–2022; (**f**) Mann-Kendall test for soil moisture. Dots indicate $p < 0.05$.

The results of the Mann–Kendall mutation test revealed that the multi-year warming trend in the basin was 0.018 °C/a (Figure 3a,d), with an abrupt change occurring around 1988: the warming rate was 0.005 °C/a during 1901–1988 and it rose to 0.019 °C/a during 1989–2022, indicating a markedly accelerated warming trend (the latter rate was approxi-

mately 3.8 times that of the former). In terms of precipitation, the multi-year wetting trend in the basin was 0.292 mm/a (Figure 3b,e), with fluctuations observed around 1975. Based on the forward and backward curve trends, this was a normal fluctuation in the data, and the overall moisturization process did not accelerate significantly. Regarding soil moisture content, the multi-year change trend in the basin was 0.0002 m^3 m^{-3}/a (Figure 3c,f), with rapid growth in the early period and a gradual stabilization in the later period. Overall, the Irtysh River basin experienced a distinct warming and wetting process during 1901–2022.

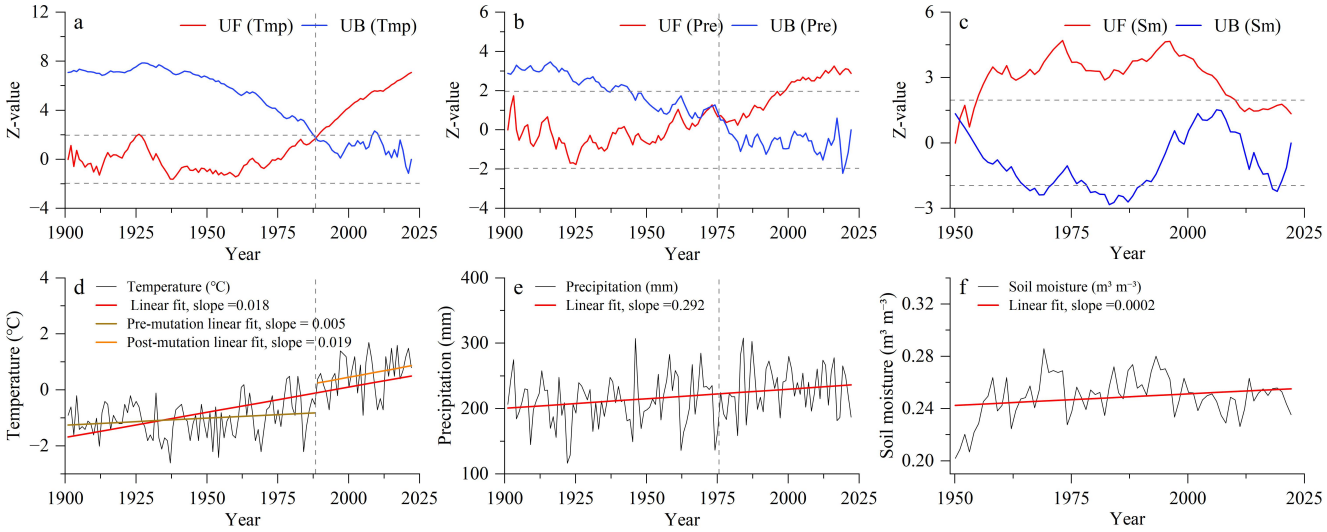


Figure 3. Mann-Kendall mutation tests and linear trends of temperature, precipitation, and soil moisture. (**a**) Mann-Kendall mutation test of temperature; (**b**) Mann-Kendall mutation test of precipitation; (**c**) Mann-Kendall mutation test of soil moisture; (**d**) linear fitting of temperature; (**e**) linear fitting of precipitation; (**f**) linear fitting of soil moisture. The horizontal dashed lines in panels (**a**–**c**) indicate the 95% confidence level, and the vertical dashed lines in panels (**d**,**e**) mark the demarcation of potential abrupt change years.

3.2. Characteristics of Vegetation Change

Based on the multi-year average NDVI values of vegetation in the study area (Figure 4a), the highest NDVI values were observed in the high-altitude northern regions, while lower values were recorded in the low-altitude southern regions, and the lowest values occurred in the mid-altitude central regions with a northwest–southeast orientation, meaning overall vegetation coverage in the central and southern regions was inferior to that in the north; the zonal mean curve in Figure 4a revealed that vegetation coverage improved with increasing latitude (evidently superior in high-latitude regions), whereas the meridional mean curve indicated moderate- and low-fluctuation variations in vegetation coverage along the longitudinal direction. Kernel density analysis (Figure 4b) showed two distinct peaks in the NDVI distribution: the first at 0.455 (representing the average NDVI level in high-value northern regions) and the second at 0.188 (corresponding to the average level in low-value southern regions). The regional average NDVI was 0.355 (minimum: 0.123; maximum: 0.629; standard deviation: 0.135); the line chart of regional average NDVI showed an increasing trend from 1982 to 2022, with a fitted line of $y = 0.0002x - 0.1019$ and a correlation coefficient (r) of 0.162, indicating a growth rate of 0.002/10a—though modest, this still reflected improved vegetation coverage in the region.

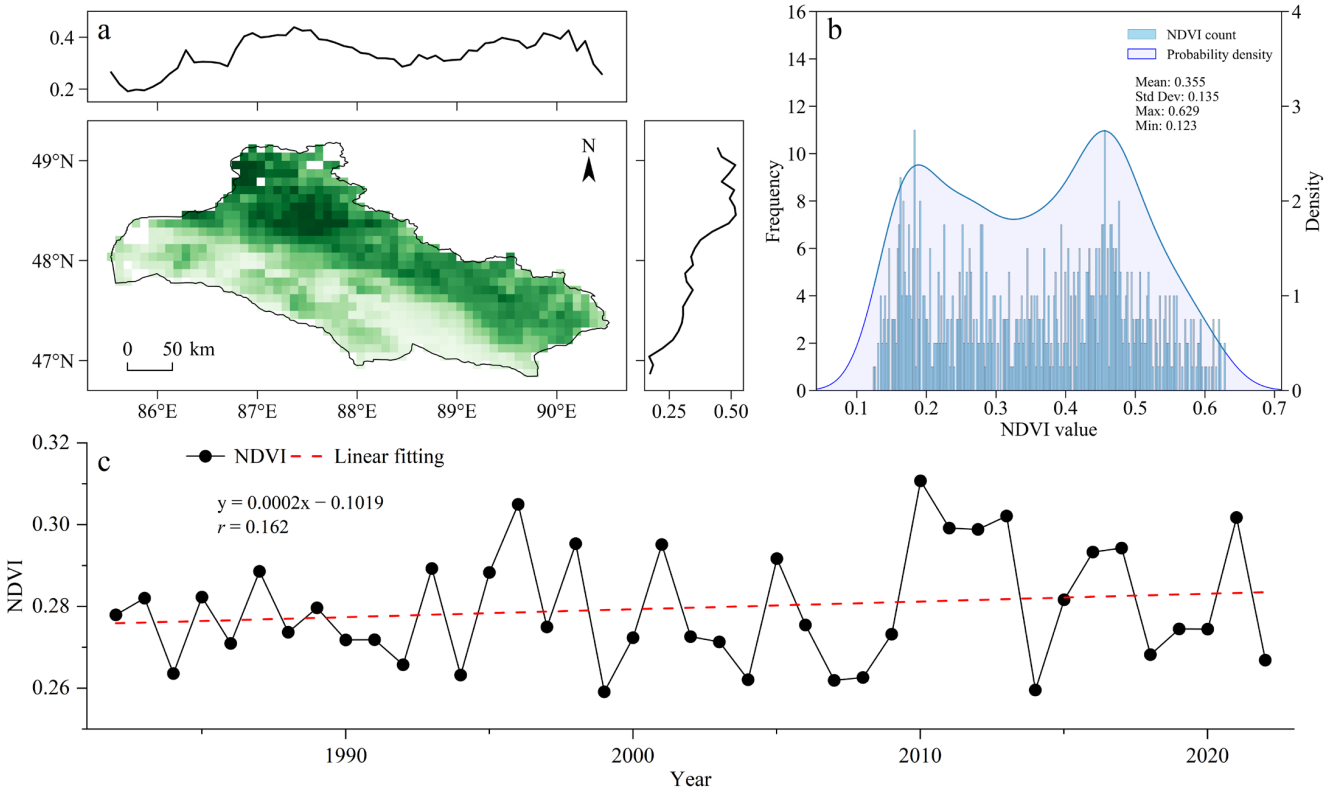


Figure 4. (**a**) Spatial distribution of average NDVI values from 1982 to 2022; (**b**) kernel density distribution of NDVI; (**c**) inter-annual variation trend of NDVI.

The vegetation distribution in the basin from 1982 to 2022 (Figure 5) showed that the main growing season of vegetation lasted from April to November, while December to March of the following year was a distinct non-growing season. April marked the germination period of vegetation growth, during which NDVI in the basin was at a relatively low level throughout the year; in May, vegetation coverage gradually spread from the south to the north, and NDVI values increased accordingly. June to August represented the annual peak period of NDVI. From September to November, vegetation in the basin showed a distinct decline, with NDVI values gradually decreasing.

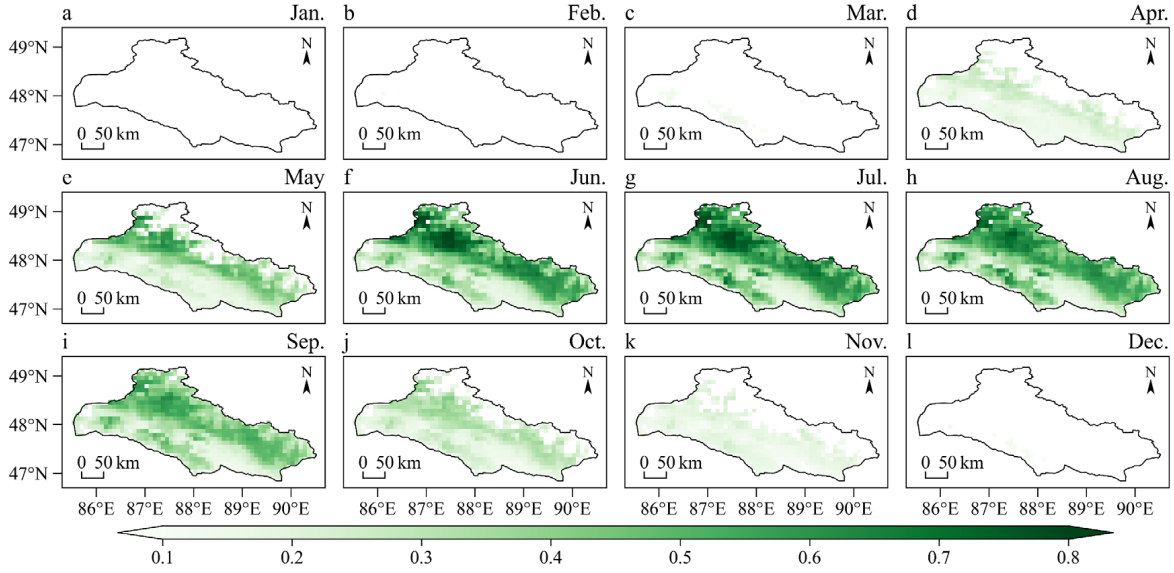


Figure 5. Spatial distribution of monthly average NDVI values from 1982 to 2022.

3.3. Response of Vegetation Growth to Climate and Hydrology

The partial correlation analysis results between monthly NDVI and simultaneous temperature, precipitation, and soil moisture content in the watershed (Figure 6a) indicate that during the early vegetation growth stage (spring, March–May), NDVI exhibits a high positive correlation with concurrent temperature compared to precipitation and soil moisture content. Specifically, the gradual warming during spring (March to May) promotes the emergence and growth of vegetation. In July and August, NDVI also exhibits significant positive correlations with both temperature and soil moisture. Taking the average values from April to May, NDVI shows a significant positive correlation with temperature. The correlation between precipitation and NDVI remains non-significant throughout this period.

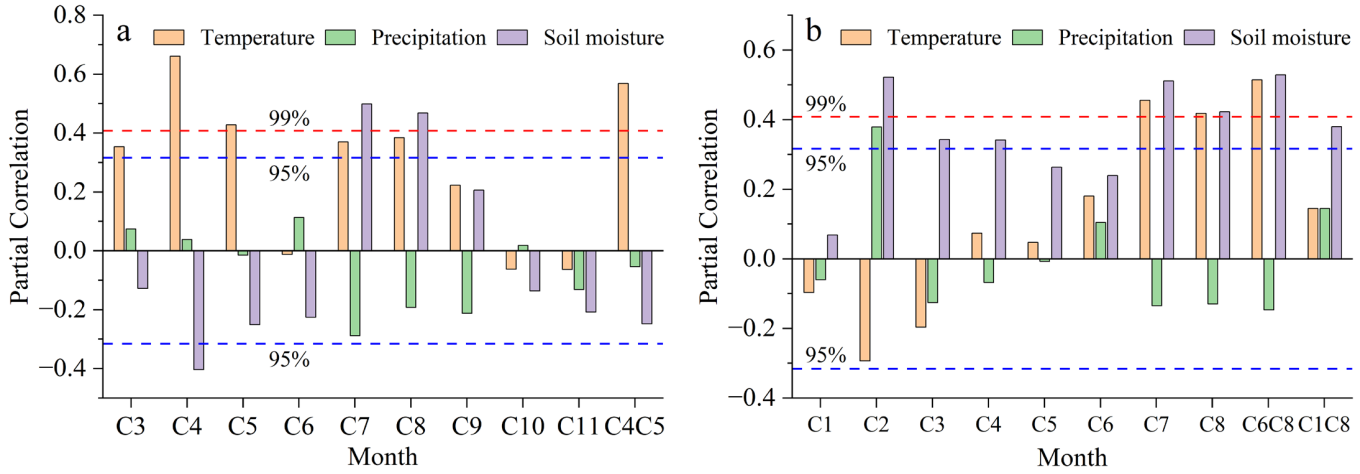


Figure 6. Partial correlation analysis between NDVI and temperature, precipitation, and soil moisture. (**a**) Partial correlation between NDVI and simultaneous temperature, precipitation and soil moisture; (**b**) partial correlation between NDVI from June to August and antecedent temperature, precipitation and soil moisture. C3 denotes March; similarly, C4C5 represent April–May, and so on.

Summer NDVI (June to August) showed positive correlations with soil moisture during the preceding period (January to May) (Figure 6b). Its correlations with temperature and precipitation were relatively weaker. The correlation between NDVI and soil moisture gradually decreased from February to May. Summer NDVI showed significant positive correlations with monthly (July and August) temperature and soil moisture, while its correlation with precipitation was weaker. Considering cumulative effects, summer NDVI also exhibited significant positive correlations with the average temperature and average soil moisture from June to August, while its association with precipitation was negative during this period. Correlations with average climatic elements from January to August indicated a significant positive correlation with soil moisture, while associations with temperature and precipitation were weaker.

Partial correlation analysis based on regional averages partially lost spatial representativeness, and the influence of climatic factors on NDVI also exhibited spatial variation. We further analyzed the spatial differences in the association between NDVI and climatic factors. Partial correlation analysis between April–May NDVI averages and corresponding temperature, precipitation, and soil moisture (Figure 7) revealed the following: Temperature was the primary driver of vegetation growth—most areas in the study region showed positive correlations (Figure 7a), with positive correlation pixels accounting for 88% (predominantly significant positive correlations) and negative correlation pixels for 12%. Regarding land cover (Figure 7d), positive correlations were observed across all five land cover types. Regarding elevation gradients (Figure 7g), NDVI showed stronger associations

with temperature below 2000 m in elevation; precipitation primarily exerted a negative influence on vegetation growth (Figure 7b), with negative correlations covering 66% of areas and positive correlations only 34%. Even when categorized by land cover and elevation (Figure 7e,h), negative correlations predominated, with only regions below 1000 m in elevation and wetland regions showing weak positive correlations. Soil moisture exhibited distinct spatial variations in its impact on vegetation growth (Figure 7c), with positive correlations covering 69% of areas and negative correlations 31%. Categorized analysis (Figure 7f,i) indicated that wetlands may show negative correlations, while most other areas exhibited positive correlations. Regions with an elevation above 2000 m exhibited relatively higher positive correlations.

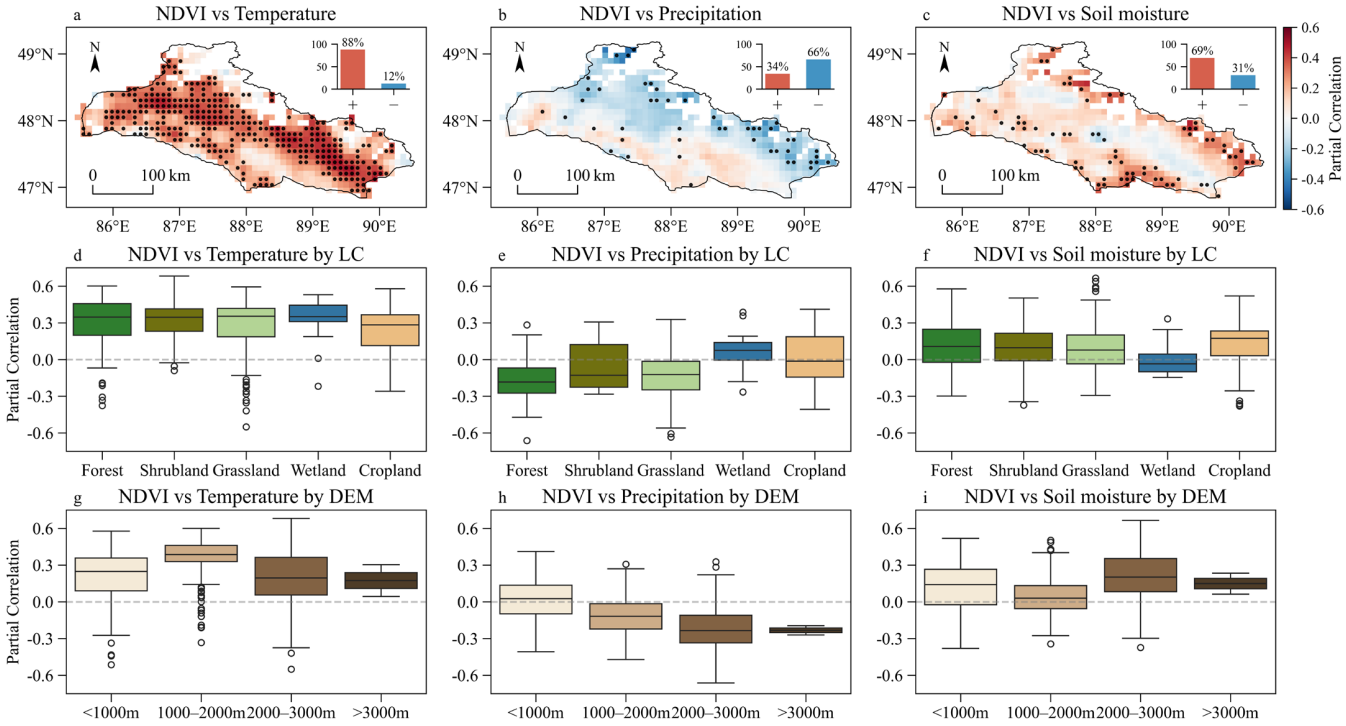


Figure 7. Spatial partial correlation analysis of NDVI averages for April–May with corresponding temperature, precipitation, and soil moisture, along with the distribution of partial correlation coefficients with land cover type and elevation. (**a**) Spatial distribution of partial correlation between NDVI and temperature; (**b**) Spatial distribution of partial correlation between NDVI and precipitation; (**c**) Spatial distribution of partial correlation between NDVI and soil moisture; (**d**) Partial correlation between NDVI and temperature across different land cover types; (**e**) Partial correlation between NDVI and precipitation across different land cover types; (**f**) Partial correlation between NDVI and soil moisture across different land cover types; (**g**) Partial correlation between NDVI and temperature across different altitude gradients; (**h**) Partial correlation between NDVI and precipitation across different altitude gradients; (**i**) Partial correlation between NDVI and soil moisture across different altitude gradients. Dots indicate $p < 0.05$.

The partial correlation analysis between the average NDVI values from June to August and temperature, precipitation, and soil moisture from January to August (Figure 8) further highlights the role of soil moisture. The impact of temperature on vegetation growth exhibits significant spatial variation (Figure 8a), with positive correlations covering 61% of the area and negative correlations accounting for 39%. Classification analysis (Figure 8d,g) indicates that wetland and cropland show higher positive correlations. Positive correlations are slightly more prevalent at 1000–3000 m elevation than at other altitudes. Precipitation primarily exerts a positive influence on vegetation growth (Figure 8b), with positive correlations covering 76% of the area and negative correlations accounting for 24%. Categorical

analysis (Figure 8e,h) reveals that positive correlations with NDVI are relatively similar across different land cover types, with slightly higher positive correlations at 1000–2000 m elevation compared to other zones. Soil moisture primarily promotes vegetation growth positively (Figure 8c), covering 72% of the area, while negative correlations account for 28%. Categorical analysis (Figure 8f,i) indicates that shrubland and grassland areas exhibit slightly higher positive correlations, while regions below 2000 m also show relatively higher positive correlations.

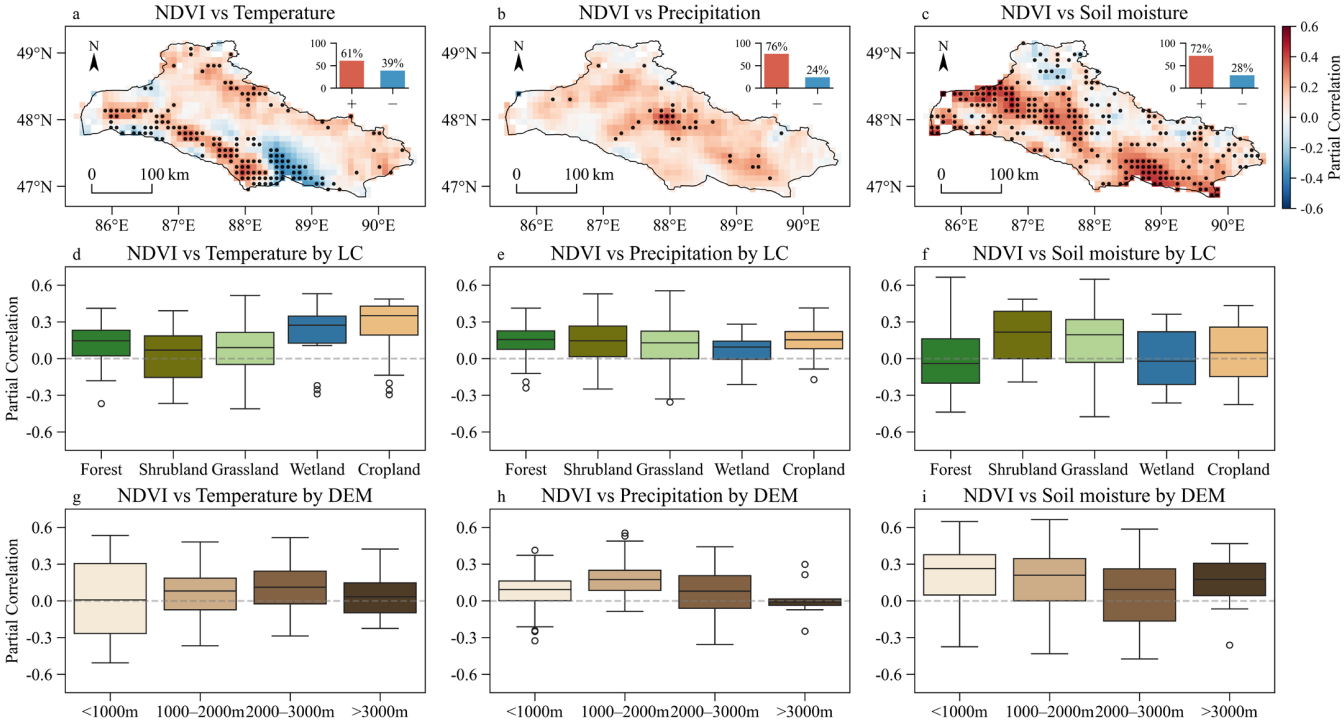


Figure 8. Spatial partial correlation analysis of NDVI averages for June–August with temperature, precipitation, and soil moisture from January to August, along with the distribution of partial correlation coefficients with land cover type and elevation. (**a**) Spatial distribution of partial correlation between NDVI and temperature; (**b**) Spatial distribution of partial correlation between NDVI and precipitation; (**c**) Spatial distribution of partial correlation between NDVI and soil moisture; (**d**) Partial correlation between NDVI and temperature across different land cover types; (**e**) Partial correlation between NDVI and precipitation across different land cover types; (**f**) Partial correlation between NDVI and soil moisture across different land cover types; (**g**) Partial correlation between NDVI and temperature across different altitude gradients; (**h**) Partial correlation between NDVI and precipitation across different altitude gradients; (**i**) Partial correlation between NDVI and soil moisture across different altitude gradients. Dots indicate $p < 0.05$.

3.4. Geographical Detection of Factors Influencing the NDVI

The factor detection results from the geographical detector (Figure 9a) reveal significant differences in the explanatory power (q-value) of various driving factors for NDVI: temperature (TEM) exhibits the strongest explanatory power (q = 0.638), followed by elevation (DEM) and soil moisture (SM). Precipitation (PRE) and land cover (LC) exhibit relatively weaker explanatory power.

Interaction detection results (Figure 9b) indicated that all factor interactions exhibited "enhancement-type" effects: the interaction between temperature and soil moisture showed the highest explanatory power (q = 0.707), with most interactions being bilinear enhancements (yellow); only the interaction between elevation and precipitation displayed a nonlinear enhancement (red, q = 0.491). This indicates that the explanatory power of NDVI through multi-factor synergistic interactions significantly exceeds that of individual

factors, reflecting the complexity of the driving mechanisms. The synergistic promotion effect of multiple climatic factors far exceeds that of other non-climatic factors.

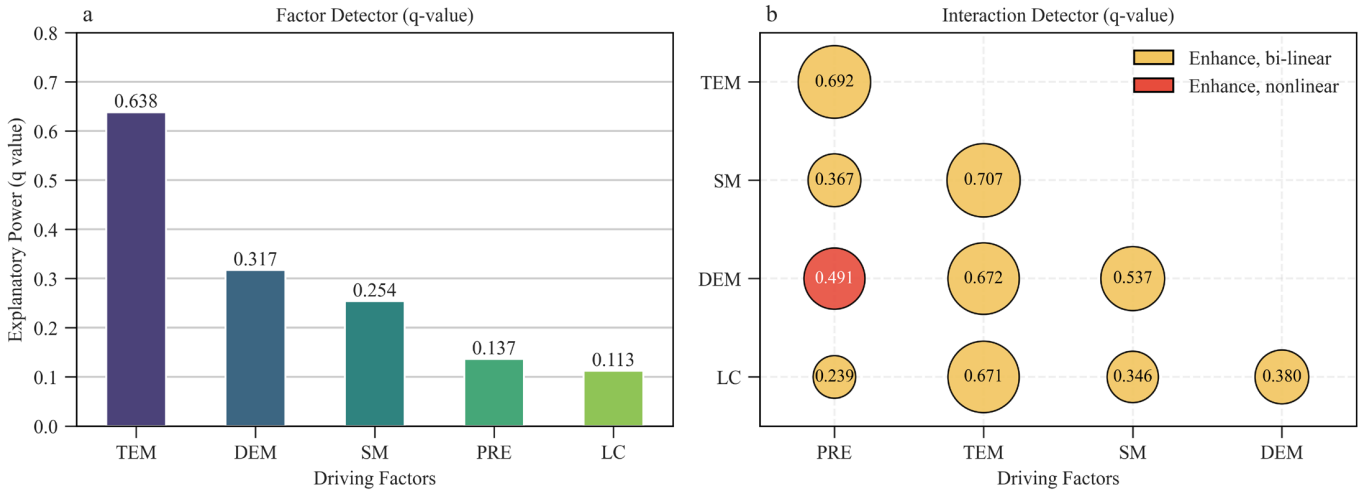


Figure 9. Individual effects of driving factors on NDVI and their interaction effects. (**a**) Factor detection of driving factors for NDVI change; (**b**) Interaction detection of driving factors for NDVI change.

3.5. Climate Fluctuation and Its Impact on Vegetation

From 1901 to 2022, the upper Irtysh River basin experienced significant warming and increased moisture, profoundly shaping regional vegetation dynamics. Spatially, higher-elevation northern areas exhibited elevated vegetation indices (NDVI) and soil moisture, while lower-elevation southern regions showed higher temperatures but reduced vegetation cover, reflecting elevation-driven redistribution of water and heat resources. Temporally, vegetation growth exhibited distinct seasonal rhythms (growing season: April–November). Spring temperatures (March–May) primarily influenced vegetation emergence and growth, while summer vegetation growth (June–August) depended on both concurrent and preceding soil moisture. The geographical detector results confirmed temperature as the strongest explanatory factor for NDVI variation (q = 0.638), followed by elevation and soil moisture.

Notably, the Mann–Kendall mutation test revealed asynchrony in climate change: temperature underwent a sharp shift around 1988 (warming rate accelerated 3.8 times), while precipitation and soil moisture showed no significant abrupt change points. This phenomenon aligned with the IPCC Sixth Assessment Report, which attributed the acceleration of global warming after the 1980s to anthropogenic greenhouse gas emissions [62]. The study area, situated in a high-latitude and high-altitude region, is susceptible to these changes. Although ERA5 shallow soil moisture data (0–7 cm) were used to study the impact on vegetation, research indicates that in arid/semi-arid regions, deep-rooted vegetation relies on deep soil moisture (>30 cm) [63]. Shallow data may have underestimated the actual available water for vegetation, thereby reducing the accuracy of NDVI–soil moisture correlation analyses.

The synergistic enhancement effect between temperature and soil moisture (q = 0.707) highlights the coupled regulatory role of the energy–water balance on vegetation. These findings guide ecological management: under ongoing climate change, differentiated strategies based on topographic gradients are needed to enhance ecosystem resilience.

3.6. Wavelet Analysis Reveals Quasi-Periodic Variations in the Vegetation–Climate System

Morlet wavelet analysis revealed that the time series of temperature (1901–2022), precipitation (1901–2022), soil moisture (1950–2022), and NDVI (1982–2022) in the basin col-

lectively exhibited certain quasi-periodic variation characteristics (Figure 10a–d). The long-term variation patterns of climate and vegetation may have been synergistically regulated by large-scale air–sea oscillations (e.g., ENSO, NAO, and AO) and changes in high-latitude circulation [64,65]. Specifically, climatic teleconnections modified the spatiotemporal distribution of regional temperature and moisture by influencing the atmospheric circulation patterns and water vapor transport processes in mid-to-high-latitude regions, thereby triggering periodic responses in the regional climate and vegetation ecosystem. Among these factors, the alternating positive and negative phases of AO and NAO were key circulation drivers of quasi-periodic fluctuations in climate and NDVI within the study area: these two oscillations regulated the intensity of the westerly belt and the southward extent of polar cold air, thereby affecting the regional heat and moisture budgets [66,67].

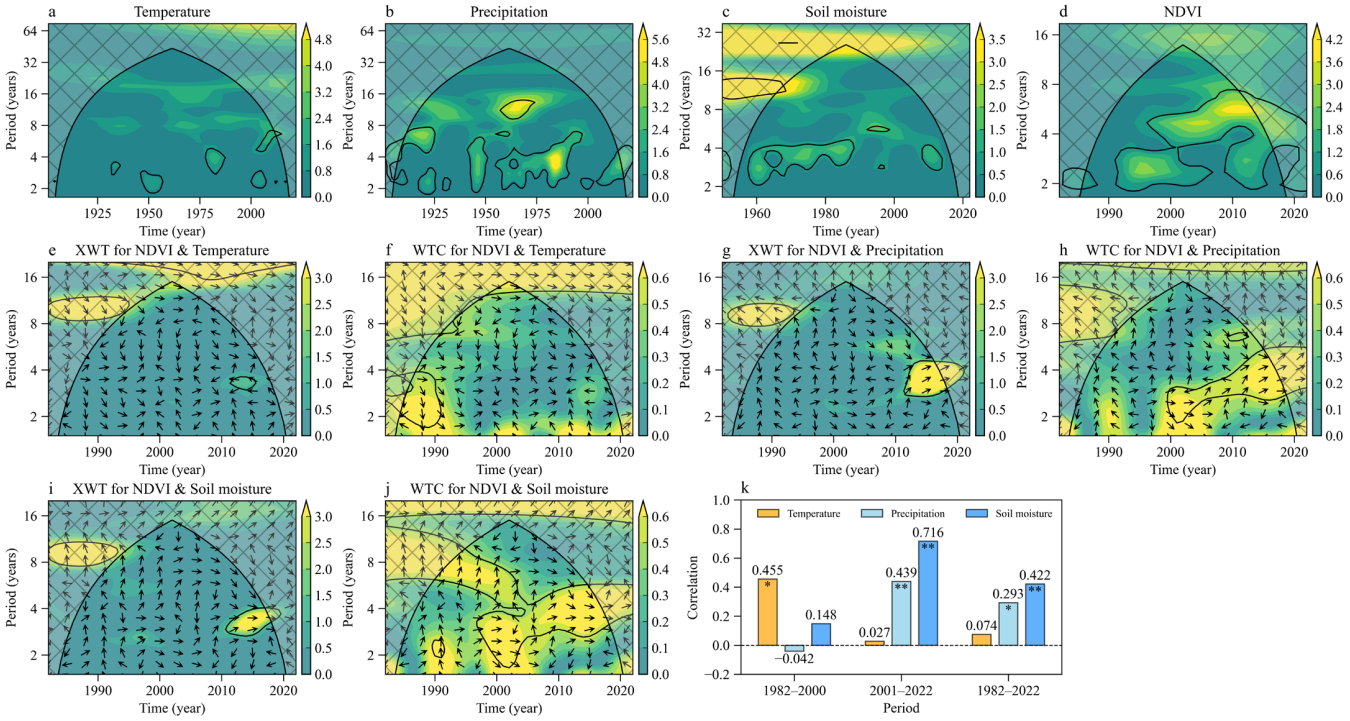


Figure 10. Wavelet analysis of NDVI with temperature, precipitation, and soil moisture. (**a**) Wavelet power spectrum of annual mean temperature; (**b**) wavelet analysis of annual total precipitation; (**c**) wavelet analysis of annual mean soil moisture; (**d**) wavelet analysis of annual mean NDVI; (**e**) cross-wavelet transform of NDVI and temperature (Jun–Aug); (**f**) wavelet coherence of NDVI and temperature (Jun–Aug); (**g**) cross-wavelet transform of NDVI and precipitation (Jun–Aug); (**h**) wavelet coherence of NDVI and precipitation (Jun–Aug); (**i**) cross-wavelet transform of NDVI and soil moisture (Jun–Aug); (**j**) wavelet coherence of NDVI and soil moisture (Jun–Aug); (**k**) correlation coefficients between NDVI from June to August and temperature, precipitation, and soil moisture in different periods. The symbol → indicates that the two variables have the same variation phase, and ← indicates the opposite variation phase. The symbol * indicates $p < 0.05$ and ** indicates $p < 0.01$.

From a periodic perspective, the 2–7-year cycle is consistent with the typical ENSO oscillation cycle, indicating that climatic and vegetation changes in this region may be influenced by teleconnections associated with anomalous sea surface temperatures in the Pacific Ocean. In contrast, the 8–15-year periodic characteristic is similar to the low-frequency variations in NAO and AO, reflecting the modulating effect of mid-to-high-latitude atmospheric circulation oscillations on the regional climate system. These multi-timescale periodic response characteristics reveal that climatic and ecosystem changes in the basin are the combined result of remote forcing from tropical air–sea interactions (e.g., ENSO) and high-latitude circulation dynamics (e.g., NAO and AO). However, there are

significant differences in the temporal spans of data for different variables (with NDVI records being the shortest at 41 years), which may reduce the ability to detect long-period signals exceeding 10 years and make it difficult to completely exclude interference from random fluctuations in short time series on cycle identification. Caution is therefore warranted when determining the driving mechanisms of periodic variations in climatic elements and NDVI.

Taking climatic elements and NDVI from June to August as an example (1982–2022), the results of cross-wavelet and wavelet coherence analysis (Figure 10e–j) indicated that the conjugate characteristics before 2000 were most pronounced for temperature, whereas those after 2000 were dominated by moisture elements (including precipitation and soil moisture). From the wavelet analysis results of temperature, the main conjugate characteristics appeared before 2000, with a quasi-period of 2–3 years (Figure 10e–f). Cross-wavelet analysis of precipitation (Figure 10g) revealed that precipitation significantly preceded NDVI during 2010–2022, indicating that precipitation promoted vegetation growth. Wavelet coherence results (Figure 10h) confirmed this relationship, which first appeared around 2000 and intensified between 2000 and 2020, indicating that precipitation became a primary driver of NDVI variations after 2000. Soil moisture (Figure 10i–j) showed similar effects on NDVI, but cross-wavelet analysis detected this influence only sporadically because of its methodological limitations. In contrast, wavelet coherence analysis showed that soil moisture maintained a positive correlation with NDVI for most of the study period.

We divided the time series into two periods (1982–2000 and 2001–2022) and analyzed correlations separately for each (Figure 10k). During 1982–2000, temperature dominated the relationship: NDVI was positively correlated with temperature ($p < 0.05$) and soil moisture, but negatively (albeit weakly) with precipitation. After 2000, moisture factors became more important. Temperature–NDVI correlations weakened, while both precipitation and soil moisture showed strong positive ($p < 0.01$) correlations with NDVI. Over the full study period, vegetation was more sensitive to moisture than to temperature, and soil moisture was the principal driver of vegetation growth and NDVI variability. This pattern is similar to other research findings; for instance, Zhang et al. (2021) found that vegetation in arid regions of northwest China responded more strongly to precipitation [68]. Moderate precipitation levels have maintained favorable soil moisture conditions.

4. Discussion

4.1. Long-Term Effects of NAO and AO on NDVI Dynamics

Figure 11a compares the variations in regional NDVI with the NAO and AO from 1982 to 2022. It shows a significant negative correlation between regional NDVI and NAO ($r = -0.529$, $p < 0.01$) and also AO ($r = -0.394$, $p < 0.05$). This finding is consistent with Liu et al.'s work on spatiotemporal vegetation patterns in the mid- and lower reaches of river basins in China, where they similarly found a negative impact of NAO on NDVI [69]. After controlling for temperature, precipitation, and soil moisture climate variables, partial correlation results indicate that a significant negative relationship persists between NDVI and NAO/AO (Figure 11b). This result indicates that the regulation of regional vegetation changes by NAO/AO is not solely mediated through local direct drivers, namely temperature, precipitation, and soil moisture conditions. They may also exert indirect effects via alternative pathways—such as modifying solar radiation (cloud cover) distribution, regulating snowpack freeze–thaw dynamics, and altering vegetation phenological rhythms—thereby reshaping the spatiotemporal patterns of regional NDVI.

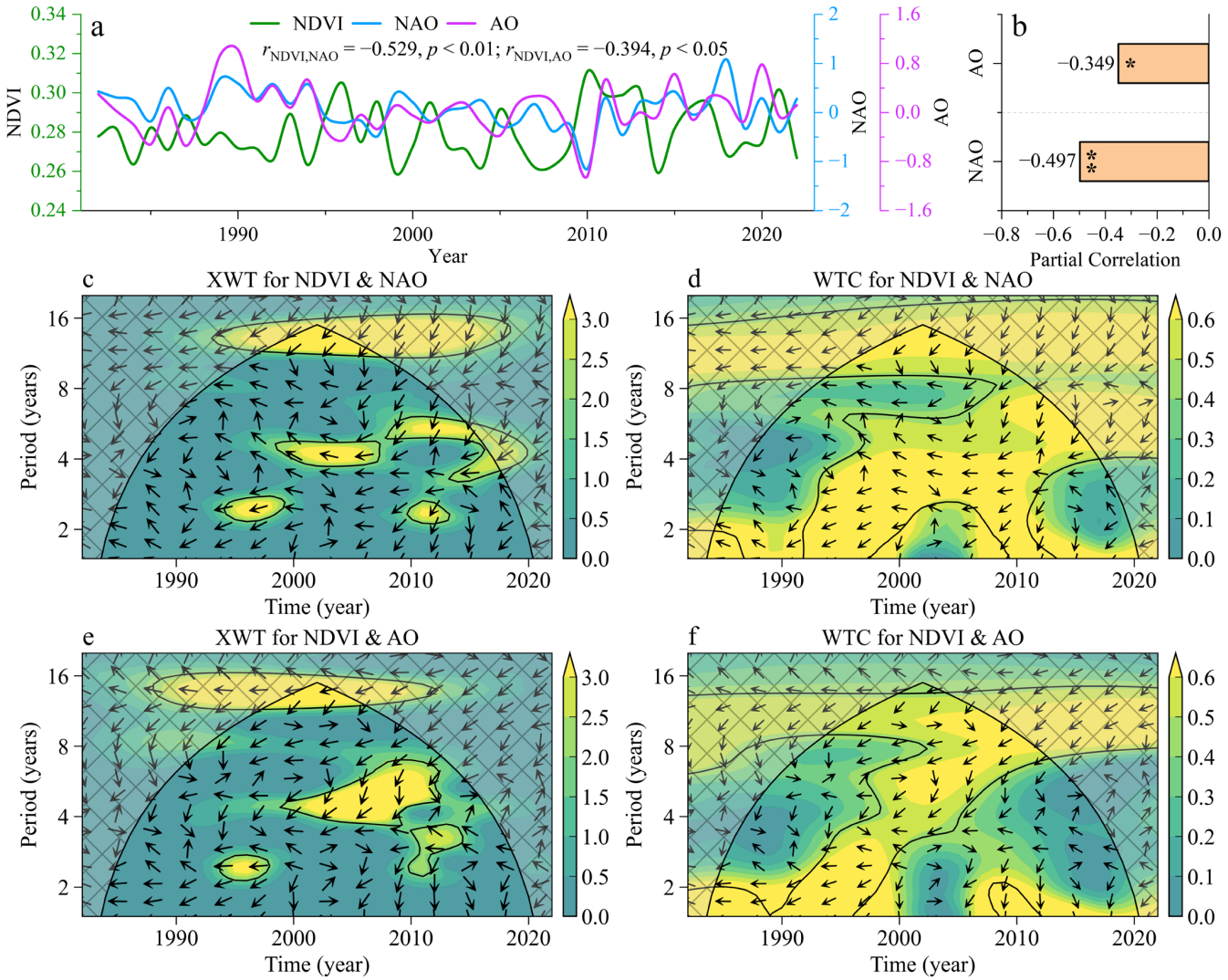


Figure 11. Comparison and wavelet analysis of NDVI with the NAO and AO indices. (**a**) Comparison of NDVI with NAO and AO; (**b**) partial correlation between NDVI and NAO, AO; (**c**) cross-wavelet transform between NDVI and NAO; (**d**) wavelet coherence between NDVI and NAO; (**e**) cross-wavelet transform between NDVI and AO; (**f**) wavelet coherence between NDVI and AO. The symbol * indicates $p < 0.05$ and ** indicates $p < 0.01$. The symbol → indicates that the two variables have the same variation phase and ← indicates the opposite variation phase.

Wavelet analysis results (Figure 11c,d) showed clear covariation patterns between NAO and NDVI at inter-annual to interdecadal scales, with an anti-phase relationship being the dominant feature: stronger positive NAO phases matched with declining regional NDVI, while stronger negative NAO phases coincided with increasing NDVI. Similarly, AO and NDVI exhibited significant covariation at inter-annual to interdecadal scales (Figure 11e,f), also with a predominantly anti-phase relationship—specifically, amplified positive AO phases coincided with reduced NDVI, while intensified negative AO phases led to an increase in NDVI. Based on correlation or partial correlation analysis and wavelet analysis results, NDVI exhibited significant long-term negative correlations with the NAO and AO, highlighting the complexity of these large-scale circulation indices in regulating regional vegetation dynamics (NDVI) over extended periods.

The study area is subject to long-term influence from westerly circulation. The multi-year average distribution characteristics of water vapor (Figure 12a) demonstrate that the impact of mid-latitude westerlies on regional water vapor transport is significantly stable; during the vegetation growing season (June–August), the sustained effect of mid-latitude westerlies

maintains a stable state of water vapor influx into the study area (Figure 12b). To further elucidate the coupling mechanism between water vapor budget and vegetation growth, this study selected five high-value years and five low-value years from the summer (June–August) NDVI average sequence during 1982–2022 and conducted a comparative analysis combining the activity characteristics of AO and NAO as well as the basin's water vapor budget status (Figure 12c,d). The results showed that during NDVI high-value years, the intensity of the mid-latitude westerly belt weakened (negative NAO phase) and shifted southward, intersecting with cold air advecting southward from the polar regions (negative AO phase).

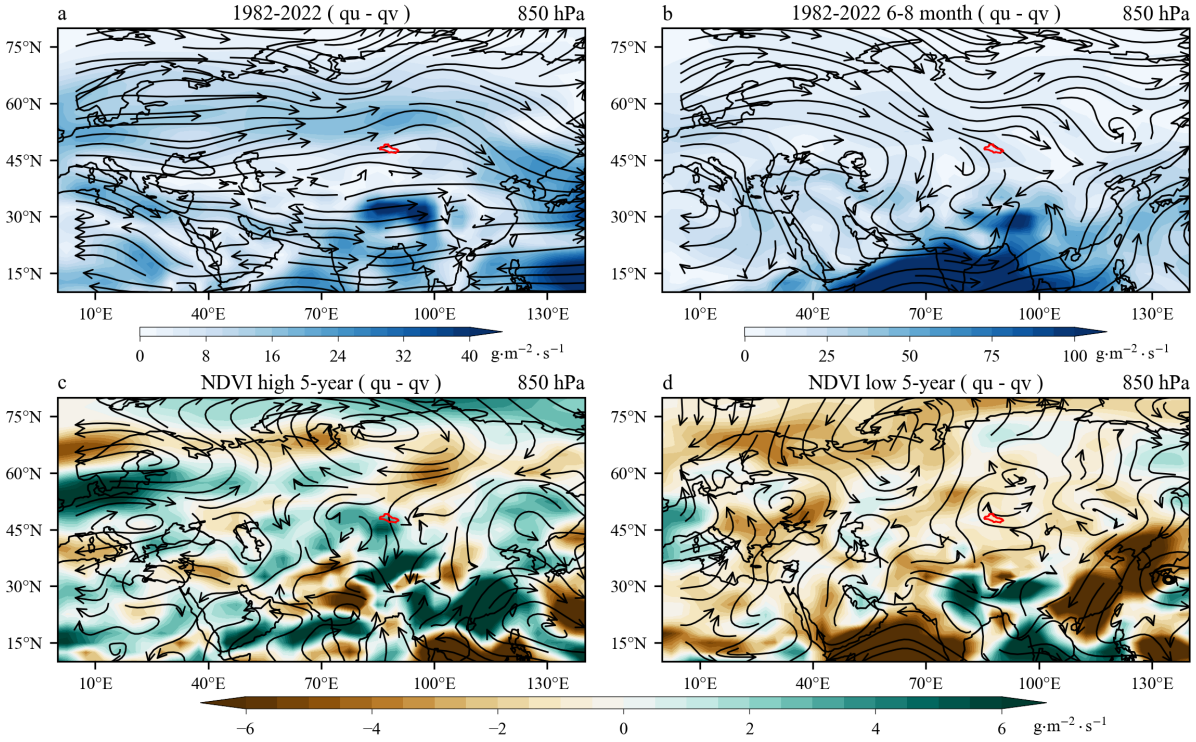


Figure 12. Water vapor budget for the annual average (1982–2022) and June–August periods, and years with extreme NDVI values (1982–2022). (**a**) Annual water vapor transport during 1982–2022; (**b**) water vapor transport in June–August during 1982–2022; (**c**) water vapor transport in the five years with extremely high NDVI values in June–August during 1982–2022; (**d**) water vapor transport in the five years with extremely low NDVI values in June–August during 1982–2022. The red circle in the figure indicates the study area and (qu−qv) represents the composite water vapor wind field result.

This moderated summer heat extremes while generating substantial precipitation, keeping soil moisture levels high throughout the growing season. Because this coincided with the basin's peak vegetation growth period, the combination of optimal temperatures and ample water supply created favorable hydrothermal conditions that greatly enhanced photosynthetic efficiency and provided strong environmental support for vegetation development. By contrast, during years with low NDVI values, the AO activity center moved northward, working in tandem with a poleward shift in the mid-latitude westerlies. This altered the water vapor sources of the basin, leading to a significant reduction in water vapor influx and subsequent insufficient local precipitation. Meanwhile, high-temperature weather from June to August intensified vegetation transpiration, causing soil moisture deficit. The imbalance in hydrothermal conditions ultimately inhibited vegetation growth.

4.2. Primary Drivers of Vegetation Greening

The upper Irtysh River basin exhibits a gradual greening trend (1982–2022 growth rate: 0.002/10a), consistent with trends observed in other Central Asian regions [54,70]. Combining

results from geographical detector analysis reveals that this greening phenomenon is primarily driven by multi-scale climatic factors, exhibiting distinct intra-annual and inter-annual patterns: Intra-annually, it follows a "temperature-dominated, moisture-sustained" pattern: warming in March–May promotes vegetation emergence, while cumulative soil moisture from January to August satisfies water demands during the growth peak (June–August). At the inter-annual level, soil moisture plays a pivotal role, while temperature and precipitation exhibit time-varying influences: before 2000, temperature exerts greater dominance (with precipitation even slightly negatively affecting vegetation when soil moisture is abundant). After 2000, precipitation surpasses temperature as the dominant factor, with soil moisture holding the strongest influence. This shift correlates with accelerated global warming in the 21st century, where warming intensifies regional transpiration, while moderate precipitation increases soil moisture, alleviating drought stress. Furthermore, as a mid-to-high-latitude arid/semi-arid region governed by the westerlies, the study area is significantly influenced by large-scale circulation indices (NAO/AO). Weakened NAO and AO enhance vegetation indices (NDVI) by altering westerly intensity and polar air incursions through alternating phase shifts, thereby regulating regional water vapor balance, temperature, and precipitation—ultimately shaping vegetation growth. It should be noted that this section focuses solely on climate drivers and excludes human impacts. Separate studies indicate that Xinjiang's vegetation has significantly improved in recent years under ecological policy support [71,72].

4.3. Implications for the Management of Agricultural and Forestry Resources

Given the pronounced warming and wetting trend and the ecological characteristic of sustained vegetation greening in the upper reaches of the Irtysh River, combined with the zonal attributes of this arid and semi-arid region, scientifically appropriate management measures can effectively maintain the balance of the local ecosystem and enhance its anti-interference and self-repair capabilities. For instance, based on the current warming and wetting development trends and while taking into account practical issues such as intensified transpiration induced by global warming since the 21st century, the moderate promotion of drought-tolerant and cold-resistant cash crops and economic forests in the study area can be carried out to improve the regional economic value on the premise of ensuring ecological adaptability. In addition, in the process of advancing agricultural development and strengthening the protection of forest resources, attention should also be paid to optimizing the planting structure and implementing moderate forest tending measures to enhance the ecosystem's capacity for water conservation, soil moisture retention, drought resistance, and disaster reduction. Blind reclamation, unreasonable forest logging, and other ecologically destructive activities must be resolutely prohibited.

4.4. Limitations and Future

Analysis in this research primarily focused on the driving effects of core climatic elements, elevation, and land cover on vegetation growth, without accounting for disturbances from human activities and extreme events (e.g., wildfires, droughts, flash floods, etc.). For instance, the upper reaches of the Irtysh River are a key region for ecological protection and economic development. Under the long-term implementation of measures such as afforestation, closed hillsides for afforestation, and the Three-North Shelterbelt Program [73], regional vegetation coverage and forest health have been improved, carbon sequestration capacity has been enhanced, and vegetation greening has been promoted, with ecological benefits gradually emerging [74,75]. Meanwhile, agricultural reclamation, water resource development, and urbanization processes have also altered the vegetation growth pattern to a certain extent. These factors do not adequately account for observed vegetation changes. Global warming has increased drought frequency and intensity in

many regions, resulting in vegetation die-off and forest degradation. Large-scale vegetation studies often miss these localized declines.

Future research should draw on NDVI and climatic datasets with finer spatial and temporal detail and expand the analysis to include factors such as human activities, socioeconomic development, and major disturbance events. The application of advanced analytical methods, including Geographically Weighted Regression (GWR) and Structural Equation Modeling (SEM), can provide a more nuanced understanding of vegetation growth dynamics in the upper Irtysh River basin. Such work would offer a stronger scientific basis for guiding vegetation conservation and ecological restoration efforts in this region.

5. Conclusions

This study employed NDVI data integrated with temperature, precipitation, soil moisture, elevation, and land cover data. Utilizing the Theil–Sen median trend estimation method, Mann–Kendall trend and mutation tests, partial correlation analysis, geographic detector, and wavelet analysis, it examined long-term warming and humidification trends in the upper Irtysh River basin. This study also described the spatiotemporal evolution characteristics of NDVI and its primary drivers, while evaluating the mechanisms through which climatic factors and atmospheric circulation influenced vegetation dynamics.

Results indicate significantly enhanced warming and humidification trends from 1901 to 2022: Spatial trend distributions reveal stronger increases in temperature and precipitation, with a slightly weaker trend in soil moisture. Regional averages indicate that annual mean temperature rose at a rate of 0.018 °C/a, with a marked acceleration in the early 1990s; annual precipitation increased at a rate of 0.292 mm/a. Measured soil moisture exhibited a steady upward trend of 0.0002 m^3 m^{-3}/a from 1950 to 2022.

From 1982 to 2022, NDVI consistently showed a greening trend of 0.002/10a, indicating overall improvement in vegetation growth conditions within the watershed. The growing season typically spans April to November, with NDVI peaks concentrated between June and August. Regarding climate responses, while precipitation and soil moisture accumulation from June to August (or January to August) ensure adequate water supply during the main growing season, the spatial patterns of these correlations align with the aforementioned responses, though they exhibit slight variations across different land cover types and elevation gradients. Geographic detector analysis reveals that temperature explains NDVI most strongly, while land cover shows the weakest explanatory power. The synergistic promotion by multiple climate factors is particularly pronounced.

On the inter-annual scale, NDVI exhibits cyclical fluctuations with climate variables ranging from 2 to 15 years, primarily regulated by atmospheric circulation. The correlation patterns from June to August further reveal a shift in climate control mechanisms: temperature is the dominant driver before 2000, after which moisture-related factors significantly increase in influence. The North Atlantic Oscillation (NAO) and Arctic Oscillation (AO) emerge as key atmospheric circulation indicators influencing vegetation variability. Both exhibit negative correlations with NDVI, with the occurrence of high- and low-NDVI phases closely linked to fluctuations in NAO and AO activity.

Author Contributions: Conceptualization, H.Z. and H.C.; methodology, H.C. and H.X.; software, H.C., and H.X.; validation, L.L., H.S. and Y.F.; formal analysis, L.L.; investigation, H.S. and Y.F.; resources, H.C. and H.Z.; data curation, H.X.; writing—original draft preparation, H.C.; writing—review and editing, H.Z., H.C., H.S., Y.F. and L.Q.; visualization, H.C. and H.X.; supervision, H.Z.; project administration, H.Z.; funding acquisition, H.Z., H.S., Y.F. and L.Q. All authors have read and agreed to the published version of the manuscript.

Funding: This research was supported by Xinjiang Natural Science Foundation General Project (2024D01A153, 202501A14), The Key Laboratory Opening Subject of Xinjiang (2025D04018), The Tianshan Talent Training Program (2023TSYCCX0089, 2024TSYCCX0041), National Natural Science Foundation of China (32061123008), S&T Development Fund of CAMS (2021KJ034), and the Practical Innovation Project of Postgraduate Students in the Professional Degree of Yunnan University (ZC-242410760).

Data Availability Statement: Data are contained within the article.

Conflicts of Interest: The authors declare no conflicts of interest.

References

1. Matthews, T.K.R.; Wilby, R.L.; Murphy, C. Communicating the Deadly Consequences of Global Warming for Human Heat Stress. *Proc. Natl. Acad. Sci. USA* **2017**, *114*, 3861–3866. [CrossRef] [PubMed]
2. Nimma, D.; Devi, O.R.; Laishram, B.; Ramesh, J.V.N.; Boddupalli, S.; Ayyasamy, R.; Tirth, V.; Arabi, A. Implications of Climate Change on Freshwater Ecosystems and Their Biodiversity. *Desalination Water Treat.* **2025**, *321*, 100889. [CrossRef]
3. Grant, L.; Vanderkelen, I.; Gudmundsson, L.; Fischer, E.; Seneviratne, S.I.; Thiery, W. Global Emergence of Unprecedented Lifetime Exposure to Climate Extremes. *Nature* **2025**, *641*, 374–379. [CrossRef]
4. Huang, J.; Yu, H.; Han, D.; Zhang, G.; Wei, Y.; Huang, J.; An, L.; Liu, X.; Ren, Y. Declines in Global Ecological Security under Climate Change. *Ecol. Indic.* **2020**, *117*, 106651. [CrossRef]
5. Phelan, J.N.; Van Houtven, G.; Clark, C.M.; Buckley, J.; Cajka, J.; Hargrave, A.; Horn, K.; Thomas, R.Q.; Sabo, R.D. Climate Change Could Negate U.S. Forest Ecosystem Service Benefits Gained through Reductions in Nitrogen and Sulfur Deposition. *Sci. Rep.* **2024**, *14*, 10767. [CrossRef] [PubMed]
6. Zhao, W.; Yu, X.; Xu, C.; Li, S.; Wu, G.; Yuan, W. Dynamic Traceability Effects of Soil Moisture on the Precipitation–Vegetation Association in Drylands. *J. Hydrol.* **2022**, *615*, 128645. [CrossRef]
7. Peng, C.; Zeng, J.; Chen, K.S.; Li, Z.; Ma, H.; Zhang, X.; Shi, P.; Wang, T.; Bi, H. Global spatiotemporal trend of satellite-based soil moisture and its influencing factors in the early 21st century. *Remote Sens. Environ.* **2023**, *291*, 113569. [CrossRef]
8. Eskandari Dameneh, H.; Gholami, H.; Telfer, M.W.; Comino, J.R.; Collins, A.L.; Jansen, J.D. Desertification of Iran in the Early Twenty-First Century: Assessment Using Climate and Vegetation Indices. *Sci. Rep.* **2021**, *11*, 20548. [CrossRef]
9. Hantson, S.; Huxman, T.E.; Kimball, S.; Randerson, J.T.; Goulden, M.L. Warming as a Driver of Vegetation Loss in the Sonoran Desert of California. *J. Geophys. Res. Biogeosci.* **2021**, *126*, e2020JG005942. [CrossRef]
10. Berveglieri, A.; Imai, N.N.; Christovam, L.E.; Galo, M.L.B.T.; Tommaselli, A.M.G.; Honkavaara, E. Analysis of Trends and Changes in the Successional Trajectories of Tropical Forest Using the Landsat NDVI Time Series. *Remote Sens. Appl. Soc. Environ.* **2021**, *24*, 100622. [CrossRef]
11. Kern, A.; Marjanović, H.; Barcza, Z. Spring Vegetation Green-up Dynamics in Central Europe Based on 20-Year Long MODIS NDVI Data. *Agric. For. Meteorol.* **2020**, *287*, 107969. [CrossRef]
12. Zhang, Y.; Ye, A. Spatial and Temporal Variations in Vegetation Coverage Observed Using AVHRR GIMMS and Terra MODIS Data in the Mainland of China. *Int. J. Remote Sens.* **2020**, *41*, 4238–4268. [CrossRef]
13. Wu, S.-T.; Chen, Y.-S. Examining Eco-Environmental Changes at Major Recreational Sites in Kenting National Park in Taiwan by Integrating SPOT Satellite Images and NDVI. *Tour. Manag.* **2016**, *57*, 23–36. [CrossRef]
14. Liu, Y.; Li, Z.; Chen, Y.; Li, Y.; Li, H.; Xia, Q.; Kayumba, P.M. Evaluation of Consistency among Three NDVI Products Applied to High Mountain Asia in 2000–2015. *Remote Sens. Environ.* **2022**, *269*, 112821. [CrossRef]
15. Lemenkova, P. SAGA GIS for Computing Multispectral Vegetation Indices by Landsat TM for Mapping Vegetation Greenness. *Contemp. Agric.* **2021**, *70*, 67–75. [CrossRef]
16. Xu, D.; Wang, C.; Chen, J.; Shen, M.; Shen, B.; Yan, R.; Li, Z.; Karnieli, A.; Chen, J.; Yan, Y.; et al. The Superiority of the Normalized Difference Phenology Index (NDPI) for Estimating Grassland Aboveground Fresh Biomass. *Remote Sens. Environ.* **2021**, *264*, 112578. [CrossRef]
17. Yu, Y.; Wang, J.; Liu, G.; Cheng, F. Forest Leaf Area Index Inversion Based on Landsat OLI Data in the Shangri-La City. *J. Indian Soc. Remote Sens.* **2019**, *47*, 967–976. [CrossRef]
18. Samadzadegan, F.; Toosi, A.; Dadrass Javan, F. A Critical Review on Multi-Sensor and Multi-Platform Remote Sensing Data Fusion Approaches: Current Status and Prospects. *Int. J. Remote Sens.* **2025**, *46*, 1327–1402. [CrossRef]
19. Rustanto, A.; Booij, M.J. Evaluation of MODIS-Landsat and AVHRR-Landsat NDVI Data Fusion Using a Single Pair Base Reference Image: A Case Study in a Tropical Upstream Catchment on Java, Indonesia. *Int. J. Digit. Earth* **2022**, *15*, 164–197. [CrossRef]
20. Li, M.; Cao, S.; Zhu, Z.; Wang, Z.; Myneni, R.B.; Piao, S. Spatiotemporally Consistent Global Dataset of the GIMMS Normalized Difference Vegetation Index (PKU GIMMS NDVI) from 1982 to 2022. *Earth Syst. Sci. Data* **2023**, *15*, 4181–4203. [CrossRef]

21. Guan, X.; Shen, H.; Wang, Y.; Chu, D.; Li, X.; Yue, L.; Li, W.; Liu, X.; Zhang, L. Fusing MODIS and AVHRR Products to Generate a Global 1-Km Continuous NDVI Time Series Covering Four Decades. *Big Earth Data* **2025**, *9*, 72–99. [CrossRef]
22. Gao, S.; Zhong, R.; Yan, K.; Ma, X.; Chen, X.; Pu, J.; Gao, S.; Qi, J.; Yin, G.; Myneni, R.B. Evaluating the Saturation Effect of Vegetation Indices in Forests Using 3D Radiative Transfer Simulations and Satellite Observations. *Remote Sens. Environ.* **2023**, *295*, 113665. [CrossRef]
23. Kaufman, Y.J.; Tanré, D.; Holben, B.N.; Markham, B.L.; Gitelson, A.A. Atmospheric Effects on the NDVI–Strategies for Its Removal. In *Proceedings of the IGARSS '92 International Geoscience and Remote Sensing Symposium*; IEEE: Piscataway, NJ, USA, 1992. [CrossRef]
24. Huete, A.R.; Liu, H.Q.; Batchily, K.; van Leeuwen, W. A Comparison of Vegetation Indices over a Global Set of TM Images for EOS-MODIS. *Remote Sens. Environ.* **1997**, *59*, 440–451. [CrossRef]
25. Huang, S.; Tang, L.; Hupy, J.P.; Wang, Y.; Shao, G. A Commentary Review on the Use of Normalized Difference Vegetation Index (NDVI) in the Era of Popular Remote Sensing. *J. For. Res.* **2021**, *32*, 1–6. [CrossRef]
26. Xu, Z.; Liu, D.; Zhao, L. Hydrothermal Conditions Modulate the Impact of Climate Extremes on Vegetation Growth in the Northern Hemisphere. *Glob. Ecol. Biogeogr.* **2024**, *33*, e13898. [CrossRef]
27. Liu, L.; Peng, J.; Li, G.; Guan, J.; Han, W.; Ju, X.; Zheng, J. Effects of Drought and Climate Factors on Vegetation Dynamics in Central Asia from 1982 to 2020. *J. Environ. Manag.* **2023**, *328*, 116997. [CrossRef]
28. Wankmüller, F.J.P.; Delval, L.; Lehmann, P.; Baur, M.J.; Cecere, A.; Wolf, S.; Or, D.; Javaux, M.; Carminati, A. Global Influence of Soil Texture on Ecosystem Water Limitation. *Nature* **2024**, *635*, 631–638. [CrossRef] [PubMed]
29. Jiao, Q.; Li, R.; Wang, F.; Mu, X.; Li, P.; An, C. Impacts of Re-Vegetation on Surface Soil Moisture over the Chinese Loess Plateau Based on Remote Sensing Datasets. *Remote Sens.* **2016**, *8*, 156. [CrossRef]
30. Jiang, N.; Shen, M.; Yang, Z. Differential Phenological Responses to Temperature among Various Stages of Spring Vegetation Green-Up. *J. Plant Ecol.* **2024**, *17*. [CrossRef]
31. Miao, L.; Jiang, C.; Xue, B.; Liu, Q.; He, B.; Nath, R.; Cui, X. Vegetation Dynamics and Factor Analysis in Arid and Semi-Arid Inner Mongolia. *Environ. Earth Sci.* **2015**, *73*, 2343–2352. [CrossRef]
32. Wilcox, K.R.; Blumenthal, D.M.; Kray, J.A.; Mueller, K.E.; Derner, J.D.; Ocheltree, T.; Porensky, L.M. Plant Traits Related to Precipitation Sensitivity of Species and Communities in Semiarid Shortgrass Prairie. *New Phytol.* **2021**, *229*, 2007–2019. [CrossRef] [PubMed]
33. Chang, Y.; Winkler, A.J.; Noori, A.; Knyazikhin, Y.; Myneni, R.B. Precipitation Leads the Long-Term Vegetation Increase in the Conterminous United States Drylands. *Environ. Res. Lett.* **2025**, *20*, 044006. [CrossRef]
34. Yu, T.; Jiapaer, G.; Bao, A.; Zheng, G.; Zhang, J.; Li, X.; Yuan, Y.; Huang, X.; Umuhoza, J. Disentangling the Relative Effects of Soil Moisture and Vapor Pressure Deficit on Photosynthesis in Dryland Central Asia. *Ecol. Indic.* **2022**, *137*, 108698. [CrossRef]
35. Radelyuk, I.; Zhang, L.; Assanov, D.; Maratova, G.; Tussupova, K. A State-of-the-Art and Future Perspectives of Transboundary Rivers in the Cold Climate—A Systematic Review of Irtysh River. *J. Hydrol. Reg. Studies* **2022**, *42*, 101173. [CrossRef]
36. Hanchu, L.; Jie, F.; Baoyin, L.; Li, W.; Qin, Q. Practical Exploration of Ecological Restoration and Management of the Mountains-Rivers-Forests-Farmlands-Lakes-Grasslands System in the Irtysh River Basin in Altay, Xinjiang. *Jore* **2021**, *12*, 766–776. [CrossRef]
37. Song, J.; Xue, Z.; Yang, B.; Liu, T.; Yuan, Y.; Xu, L.; Zhang, Z. Spatial Distribution Patterns and Influencing Factors of Dominant Species in Plain Valley Forests of the Irtysh River Basin. *Forests* **2024**, *15*, 1237. [CrossRef]
38. Li, Y.; Xue, Z.; Liu, T.; Song, J.; Yuan, Y.; Xu, L.; Zhang, Z. Genetic Diversity of Dominant Species Betula pendula in River Valley Forests in the Irtysh River Basin and Sustainable Conservation Measures for the Future. *Sustainability* **2024**, *16*, 3217. [CrossRef]
39. Fan, X.; Qu, Y.; Zhang, J.; Bai, E. China's Vegetation Restoration Programs Accelerated Vegetation Greening on the Loess Plateau. *Agric. For. Meteorol.* **2024**, *350*, 109994. [CrossRef]
40. Li, X.; Wang, K.; Huntingford, C.; Zhu, Z.; Peñuelas, J.; Myneni, R.B.; Piao, S. Vegetation Greenness in 2023. *Nat. Rev. Earth Environ.* **2024**, *5*, 241–243. [CrossRef]
41. Ma, Y.; Ren, J.; Kang, S.; Niu, J.; Tong, L. Spatial-Temporal Dynamics of Meteorological and Agricultural Drought in Northwest China: Propagation, Drivers and Prediction. *J. Hydrol.* **2025**, *650*, 132492. [CrossRef]
42. Chen, X.; Chen, T.; He, B.; Liu, S.; Zhou, S.; Shi, T. The Global Greening Continues despite Increased Drought Stress since 2000. *Glob. Ecol. Conserv.* **2024**, *49*, e02791. [CrossRef]
43. Peng, S.; Ding, Y.; Liu, W.; Li, Z. 1 km monthly temperature and precipitation dataset for China from 1901 to 2017. *Earth Syst. Sci. Data* **2019**, *11*, 1931–1946. [CrossRef]
44. Peng, S. *1-km Monthly Precipitation Dataset for China (1901–2024)*; National Tibetan Plateau/Third Pole Environment Data Center: Beijing, China, 2020. [CrossRef]
45. Peng, S. *1-km Monthly Mean Temperature Dataset for China (1901–2024)*; National Tibetan Plateau/Third Pole Environment Data Center: Beijing, China, 2019. [CrossRef]
46. Wu, B.; Zhang, Y.; Wang, Y.; He, Y.; Wang, J.; Wu, Y.; Lin, X.; Wu, S. Mitigation of Urban Heat Island in China (2000–2020) through Vegetation-Induced Cooling. *Sustain. Cities Soc.* **2024**, *112*, 105599. [CrossRef]

47. Feng, H.; Kang, P.; Deng, Z.; Zhao, W.; Hua, M.; Zhu, X.; Wang, Z. The Impact of Climate Change and Human Activities to Vegetation Carbon Sequestration Variation in Sichuan and Chongqing. *Environ. Res.* **2023**, *238*, 117138. [CrossRef]
48. Zhang, J.; Yang, T.; Deng, M.; Huang, H.; Han, Y.; Xu, H. Spatiotemporal Variations and Its Driving Factors of NDVI in Northwest China during 2000–2021. *Environ. Sci. Pollut. Res.* **2023**, *30*, 118782–118800. [CrossRef]
49. Xue, C.; Zan, M.; Zhou, Y.; Li, K.; Zhou, J.; Yang, S.; Zhai, L. Solar-Induced Chlorophyll Fluorescence-Based GPP Estimation and Analysis of Influencing Factors for Xinjiang Vegetation. *Forests* **2024**, *15*, 2100. [CrossRef]
50. Lal, P.; Singh, G.; Das, N.N.; Colliander, A.; Entekhabi, D. Assessment of ERA5-Land Volumetric Soil Water Layer Product Using In Situ and SMAP Soil Moisture Observations. *IEEE Geosci. Remote Sens. Lett.* **2022**, *19*, 2508305. [CrossRef]
51. Huang, W.; Chen, F.; Feng, S.; Chen, J.; Zhang, X. Interannual Precipitation Variations in the Mid-Latitude Asia and Their Association with Large-Scale Atmospheric Circulation. *Chin. Sci. Bull.* **2013**, *58*, 3962–3968. [CrossRef]
52. Jiang, N.; Yan, Q.; Xu, Z.; Shi, J.; Zhang, R. The Meridional Shift of the Midlatitude Westerlies over Arid Central Asia during the Past 21 000 Years Based on the TraCE-21ka Simulations. *J. Clim.* **2020**, *33*, 7455–7478. [CrossRef]
53. Lavagnini, I.; Badocco, D.; Pastore, P.; Magno, F. Theil–Sen Nonparametric Regression Technique on Univariate Calibration, Inverse Regression and Detection Limits. *Talanta* **2011**, *87*, 180–188. [CrossRef] [PubMed]
54. Zhang, H.; Li, L.; Zhao, X.; Chen, F.; Wei, J.; Feng, Z.; Hou, T.; Chen, Y.; Yue, W.; Shang, H.; et al. Changes in Vegetation NDVI and Its Response to Climate Change and Human Activities in the Ferghana Basin from 1982 to 2015. *Remote Sens.* **2024**, *16*, 1296. [CrossRef]
55. Li, Y.; He, Y.; Zhang, Y.; Jia, L. Spatiotemporal Evolutionary Analysis of Rainfall Erosivity during 1901–2017 in Beijing, China. *Environ. Sci. Pollut. Res.* **2022**, *29*, 2510–2522. [CrossRef]
56. Chen, P.; Pan, H.; Xu, Y.; He, W.; Yao, H. Spatial-Temporal Evolution Characteristics and Driving Force Analysis of NDVI in Hubei Province, China, from 2000 to 2022. *Forests* **2024**, *15*, 719. [CrossRef]
57. Wang, J.; Zhang, T.; Fu, B. A Measure of Spatial Stratified Heterogeneity. *Ecol. Indic.* **2016**, *67*, 250–256. [CrossRef]
58. Daubechies, I. The Wavelet Transform, Time-Frequency Localization and Signal Analysis. *IEEE Trans. Inf. Theory* **1990**, *36*, 961–1005. [CrossRef]
59. Torrence, C.; Compo, G.P. A Practical Guide to Wavelet Analysis. *Bull. Am. Meteorol. Soc.* **1998**, *79*, 61–78. [CrossRef]
60. Maraun, D.; Kurths, J. Cross Wavelet Analysis: Significance Testing and Pitfalls. *Nonlinear Process. Geophys.* **2004**, *11*, 505–514. [CrossRef]
61. Farzana, S.Z.; Paudyal, D.R.; Chadalavada, S.; Alam, M.J. Spatiotemporal Variability Analysis of Rainfall and Water Quality: Insights from Trend Analysis and Wavelet Coherence Approach. *Geosciences* **2024**, *14*, 225. [CrossRef]
62. Lee, H.; Calvin, K.; Dasgupta, D.; Krinner, G.; Mukherji, A.; Thorne, P.; Trisos, C.; Romero, J.; Aldunce, P.; Barrett, K.; et al. *Climate Change 2023: Synthesis Report. Contribution of Working Groups I, II and III to the Sixth Assessment Report of the Intergovernmental Panel on Climate Change*; IPCC: Geneva, Switzerland, 2023.
63. Khanal, P.; Hoek Van Dijke, A.J.; Schaffhauser, T.; Li, W.; Paulus, S.J.; Zhan, C.; Orth, R. Relevance of Near-Surface Soil Moisture vs. Terrestrial Water Storage for Global Vegetation Functioning. *Biogeosciences* **2024**, *21*, 1533–1547. [CrossRef]
64. Li, H.; Fan, K. Dominant Patterns of Winter Surface Temperature over Central Asia and Their Connection with Atmospheric Circulation. *Atmos. Ocean. Sci. Lett.* **2022**, *15*, 100210. [CrossRef]
65. Yan, X.; Zhang, Q.; Ren, X.; Wang, X.; Yan, X.; Li, X.; Wang, L.; Bao, L. Climatic Change Characteristics towards the "Warming–Wetting" Trend in the Pan-Central-Asia Arid Region. *Atmosphere* **2022**, *13*, 467. [CrossRef]
66. Zhuang, Y.; Zhang, J.; Wu, L. Linkages of Surface Temperature Variations over Central Asia with Large-Scale Climate Patterns. *Theor. Appl. Climatol.* **2021**, *145*, 197–214. [CrossRef]
67. Tang, W.; Xiao, F.; Lai, S. Multi-Temporal Variabilities of Extreme Precipitation over Central Asia and Associated Planetary-Scale Climate Modes. *Atmosphere* **2023**, *14*, 1300. [CrossRef]
68. Zhang, Q.; Yang, J.; Wang, W.; Ma, P.; Lu, G.; Liu, X.; Yu, H.; Fang, F. Climatic Warming and Humidification in the Arid Region of Northwest China: Multi-Scale Characteristics and Impacts on Ecological Vegetation. *J. Meteorol. Res.* **2021**, *35*, 113–127. [CrossRef]
69. Liu, J.; Fu, J.; Qin, J.; Su, B.; Hong, Y. Effects of Climate Variability and Urbanization on Spatiotemporal Patterns of Vegetation in the Middle and Lower Yangtze River Basin, China. *Front. Plant Sci.* **2024**, *15*, 1459058. [CrossRef]
70. Luo, M.; Sa, C.; Meng, F.; Duan, Y.; Liu, T.; Bao, Y. Assessing Extreme Climatic Changes on a Monthly Scale and Their Implications for Vegetation in Central Asia. *J. Clean. Prod.* **2020**, *271*, 122396. [CrossRef]
71. Li, G.; Liang, J.; Wang, S.; Zhou, M.; Sun, Y.; Wang, J.; Fan, J. Characteristics and Drivers of Vegetation Change in Xinjiang, 2000–2020. *Forests* **2024**, *15*, 231. [CrossRef]
72. Guan, J.; Yao, J.; Li, M.; Zheng, J. Assessing the Spatiotemporal Evolution of Anthropogenic Impacts on Remotely Sensed Vegetation Dynamics in Xinjiang, China. *Remote Sens.* **2021**, *13*, 4651. [CrossRef]
73. Zhang, C.; Yao, X.; Wang, G.; Jin, H.; Sha, T.; Chu, X.; Zhang, J.; Cao, J. Temporal and Spatial Variation of Land Use and Vegetation in the Three–North Shelter Forest Program Area from 2000 to 2020. *Sustainability* **2022**, *14*, 16489. [CrossRef]

74. Quanqin, S.; Jiangwen, F.; Jiyuan, L.; Fan, Y.; Hua, L.; Xiuchun, Y.; Mingxiang, X.; Peng, H.; Xingjian, G.; Lin, H. Approaches for Monitoring and Assessment of Ecological Benefits of National Key Ecological Projects. *Adv. Earth Sci.* **2017**, *32*, 1174. [CrossRef]
75. Li, Z.; Wang, S.; Li, C.; Ye, C.; Gao, D.; Chen, P. The Trend Shift Caused by Ecological Restoration Accelerates the Vegetation Greening of China's Drylands since the 1980s. *Environ. Res. Lett.* **2022**, *17*, 044062. [CrossRef]

Disclaimer/Publisher's Note: The statements, opinions and data contained in all publications are solely those of the individual author(s) and contributor(s) and not of MDPI and/or the editor(s). MDPI and/or the editor(s) disclaim responsibility for any injury to people or property resulting from any ideas, methods, instructions or products referred to in the content.